Biosensors and Bioelectronics 146 (2019) 111731

Contents lists available at ScienceDirect

Biosensors and Bioelectronics

journal homepage: http://www.elsevier.com/locate/bios

Electroanalysis of isoniazid and rifampicin: Role of nanomaterial electrode modifiers

Aref Farokhi-Fard [a], Behrouz Golichenari [b], Mahdi Mohammadi Ghanbarlou [c], Saeed Zanganeh [d,e], Farzam Vaziri [f,g,*]

[a] Biotechnology Research Center, Pasteur Institute of Iran, Tehran, 1316943551, Iran
[b] Department of Pharmaceutical Biotechnology, School of Pharmacy, Mashhad University of Medical Sciences, Mashhad, 9177899191, Iran
[c] National Cell Bank of Iran, Pasteur Institute of Iran, Tehran, 1316943551, Iran
[d] Department of Hematology and Medical Laboratory Sciences, Faculty of Allied Medicine, Kerman University of Medical Sciences, Kerman, 7616913555, Iran
[e] Department of Nanobiotechnology, Advanced Technology Group, Pasteur Institute of Iran, Tehran, 1316943551, Iran
[f] Department of Mycobacteriology and Pulmonary Research, Pasteur Institute of Iran, Tehran, 1316943551, Iran
[g] Microbiology Research Center (MRC), Pasteur Institute of Iran, Tehran, 1316943551, Iran

ARTICLE INFO

Keywords:
Hepatotoxicity
Isoniazid
Rifampicin
Electroanalysis
Nanomaterial
Electrode modifier

ABSTRACT

Thanks to operational simplicity, speediness, possibility of miniaturization and real-time nature, electrochemical sensing is a supreme alternative for non-electrochemical methodologies in drug quantification. This review, highlights different nanotech-based sensory designs for electroanalysis of isoniazid and rifampicin, the most important medicines for patients with tuberculosis. We first, concisely mention analyses with bare electrodes, associated impediments and inspected possible strategies and then critically review the last two decades works with focus on different nano-scaled electrode modifiers. We organized and described the materials engaged in several categories: Surfactants modifiers, polymeric modifiers, metallic nanomaterials, carbon based nano-modifiers (reduced graphene oxide, multi-walled carbon nanotubes, ordered mesoporous carbon) and a large class of multifarious nano composites-based sensors and biosensors. The main drawbacks and superiorities associated with each array as well as the current trend in the areas is attempted to discuss. Summary of 79 employed electrochemical approaches for analysis of isoniazid and rifampicin has also been presented.

1. Introduction

Tuberculosis (TB), one of the top ten causes of human death, afflict approximately 10 million people every year. Around 1.3 million HIV-negative individuals and 374,000 HIV-positive people died from TB in 2016. Based on global tuberculosis report 2017, Treatment regimen usually administered for patients with susceptible strains, include isoniazid (INZ), rifampicin (RIF), pyrazinamide (PZM) and ethambutol (ETB) for 2 months, followed by "continuation phase" (INZ + RIF for 4 months). The two first line anti-tuberculosis drugs, INZ and RIF, are usually the most prescribed drugs for TB patients as well on the WHO's list of essential medicines.

Hepatotoxicity associated with INZ and RIF, can even be more disastrous than viral hepatitis (Ramappa and Aithal, 2013). To avoid such lethal adverse effects, development of reliable, simple, rapid and selective analytical methods is highly crucial for accurate measurement of these two medications in biological fluids as well as in quality control process of pharmaceutical preparations (Thapliyal et al., 2015).

Because of its operational simplicity, rapidity and real-time detection possibility, electrochemical sensors could be worthy tools for this purpose. However, bare electrodes exhibited large over-potential and low sensitivity and selectivity (Lima et al., 2016). Modification of electrodes with nanomaterials, can greatly improve the electrochemical response (Jena and Raj, 2010, Asadpour-Zeynali and Mollarasouli, 2017). In this review, we first present a brief description of INZ and RIF and then deeply focus in nano-structured electrode modifiers that have been investigated in the last two decades.

2. General description of INZ and RIF

Isoniazid (isonicotinic acid hydrazide or pyridine-4-carboxylic acid hydrazide, abbreviated as IZ, INH or INZ), the most prescribed drug in

* Corresponding author. Department of Mycobacteriology and Pulmonary Research, Pasteur Institute of Iran, P. O. box: 1316943551, Tehran, Iran.
E-mail addresses: f_vaziri@pasteur.ac.ir, farzam_vaziri@yahoo.com (F. Vaziri).

https://doi.org/10.1016/j.bios.2019.111731
Received 14 August 2019; Received in revised form 22 September 2019; Accepted 23 September 2019
Available online 4 October 2019

tuberculosis, was first synthesized in 1912 (Rozwarski et al., 1998; Chouchane et al., 2000). INZ is a lipophilic molecule ($pK_a = 1.8$, 3.5 and 10.8 related to hydrazine nitrogen, pyridine nitrogen, and acidic group respectively) (Lund, 1994), therefore, at acidic pH, charged positively (Atta et al., 2011a,b).

In liver, INZ is metabolized to its biologically inactive form, acetyl isoniazid (AcINZ) (El-Yazigi and Raines, 1992). INZ have a peak time (T_{max}) of 1–2 h and urinary drug elimination of 75–95 percent (Thapliyal et al., 2015). INZ seems to be activated by a catalase-peroxidase named KatG in susceptible strains. This reaction leads to formation of nicotinoyl-NAD complex which can tightly bind to enoyl-acyl carrier protein reductase (INZ A) and eventually block the fatty acid synthase (Suarez et al., 2009). Consequently, the drug exerts its mycobacteriostatic activity against slow replicating bacilli through inhibiting the biosynthesis of mycolic acid, a vital moiety of Mtb cell wall (Winder and Collins, 1970; Wei et al., 2003; Madan et al., 2005). Besides, interferences with the metabolism of bacterial proteins, nucleic acids, carbohydrates and lipids have been proposed as mechanisms for anti-mycobacterial activity of INZ. Bacteriostatic or bactericidal activity of INZ depends on the concentration of the drug at the site of infection as well as the susceptibility of the agent (Notterman et al., 1986; Tafazoli et al., 2008).

In spite of the valuable effects of INZ, it can cause several lethal side effects. It has been shown that INZ can induce lung tumor formation in mice (Maru and Bhide, 1982) as well as development of systemic lupus erythematosus especially after long-term therapy (Rubin, 2005). INZ induced hepatotoxicity which attributed to its major drug metabolite, hydrazine (HZN), is frequently seen in patients who intake high doses (Tafazoli et al., 2008), particularly in slow metabolizers (Ajayi et al., 2016).

Rifampicin (3-[(4-methyl-l-piperazinyl)imino]methyl rifamycin SV, AKA rifaldazine or rifampin, abbreviated as R, RA, RF, or RIF) with the formula of $C_{43}H_{58}N_7O_{12}$, was discovered in 1965, and approved in the US in 1971 (SANDERS, 1976; Sensi, 1983, Ty et al. 2016). RIF is a polyketide belonging to ansamycins, which exerts its antibacterial activity via inhibiting bacterial DNA-dependent RNA polymerase (Calvori et al., 1965) through binding to the pocket of the RNA polymerase β subunit within the DNA/RNA channel (Campbell et al., 2001). RIF is an amphoteric drug ($pK_{a1} = 1.7$ for 4 hydroxyl group and $pK_{a2} = 7.9$ based on 3-piperazine nitrogen) (Asadpour-Zeynali and Mollarasouli, 2017).

It is constantly used to treat tuberculous and non-tuberculous (*Mycobacterium leprae* and *Mycobacterium kansasii)* mycobacterial infections (Gilbert, 2011). It has also been approved for treatment of asymptomatic carriers of *Neisseria meningitides* (SANDERS, 1976). RIF combination therapies is also sometimes used against non-mycobacteria such as *Legionella pneumophila* (Varner et al., 2011), methicillin-resistant *Staphylococcus aureus* (MRSA) (Forrest and Tamura, 2010) and moreover as chemoprophylaxis against Brucellosis and also against meningitis caused by *Streptococcus pneumoniae*, *Haemophilus influenzae* Type b and *Neisseria meningitides* (Shane, 2006; Mola et al., 2008).

RIF is absorbed rapidly from the gastrointestinal tract. For therapeutic drug monitoring (TDM) of RIF, a 2-h post-dose sample is suggested. At this time, Orally administered RIF approaches its peak plasma concentration (Chawla et al., 2016). Almost all of the drug is metabolized by the liver to its microbiologically active form, deacetylrifampin, DARIF (El-Yazigi and Raines, 1992) and finally excreted through the feces (60–65%) and urine (about 30%). About 7% of the administered RIF is eliminated intact via the urine. The drug has a half-life of 1.5–5.0 h, in healthy individuals. Liver dysfunction can greatly increase this time (Rana, 2013). RIF is a potent inducer of many of cytochrome P450 superfamily members (Rana, 2013). As a result, it can remarkably reduce the effects of many drugs (such as oral contraceptives (Shane, 2006), warfarin (Stockley, 1994) and antiretroviral agents (Control and Prevention, 2000)) through elevating their metabolic rate (Collins, 1985). For these reason, regular liver function examinations are usually needed due to RIF associated hepatotoxicity (Chang et al., 1997).

3. Applicability of sensors for INZ and RIF determination

Anti-tubercular medications associated hepatic damage can be more dangerous than that of acute viral hepatitis (Ramappa and Aithal, 2013). INZ is supposed to have more toxic effect on liver and co-administration of this drug with RIF increases the rate of hepatotoxicity (Chang et al., 2007). Due to their small therapeutic windows, the plasma levels of INZ and RIF must be tightly and repeatedly controlled by using a reliable tool to achieve a more effective treatment, avoid adverse reactions and improve the life quality of patients. Therefore, development of a low-cost, simple, rapid, selective, sensitive and portable analytical method is very essential to accurate measurement of INZ and RIF in biological fluids as well as to use in quality control process of pharmaceutical preparations.

Six decades ago, researchers developed some colorimetric tests for INZ determination with different strategies. Naphthoquinone–mercuric chloride (N-M) test for example, was based on Schiff`s base formation between INZ and naphthoquinone and utilized $HgCl_2$ for detection of the resulted product (Gangadharam et al., 1958). High detection limit (10–50 μg/ml for example in N-M test), however, was the major shortcoming of these tests, even in improved versions (Korrapati et al., 2017). This drawback necessitates the use of large sample volumes for decisive determination of the analyte. In the United States Pharmacopeia (USP 41, 2018), HPLC has been declared for the determination of INZ and RIF in pharmaceuticals. Up to now, many flurimetric, titrimetric, chromatographic and spectrometric approaches have been applied to detect INZ and RIF (Table 1). Although each of these methods have their own advantages, however, they are mostly laborious, time consuming and need sophisticated infrastructure, un-portable facilities and multifaceted pretreatment (extraction and derivatization steps, pH adjustment, adding of diluent or unstable oxidants) by high pure solvent or reagents. (Nagaraja et al., 1996; Lapa et al., 2000; Zhang et al., 2008). Sensing methods instead are simple, fast and real-time in nature and generally deal with transportable instruments which could detect the analyte(s) with high sensitivity and selectivity without or with minimum pretreatment steps.

4. Electroanalysis of INZ and RIF

Several sensing procedures have been reported to date for analysis of INZ and RIF including mass-sensitive quartz crystal microbalance (QCM)-based sensors (Bano et al., 2019; Munawar et al., 2019), chemiluminescence-based sensors (Song et al., 2001; Xiong et al., 2007), membrane-based optical sensors (Safavi et al., 2008), etc. Based on the literatures, however, the most popular devices are electrochemical sensors.

4.1. Electroanalysis with bare electrodes, related impediments and possible approaches

In early efforts especially, a number of electrochemical investigations by unmodified electrodes has been performed for analysis of INZ and RIF. The examples include adsorptive stripping voltammetry (AdSV) at hanging mercury drop electrode (HMDE) for the determination of RIF (Lomillo et al., 2002) and INZ (Ghoneim et al., 2003), use of carbon paste electrode (CPE) for simultaneous determination of RIF and INZ by AdSV (Hammam et al., 2004), differential pulse voltammetry (DPV) with gold electrode for the determination of INZ (Yun Xia and Ya Hu, 2005), Use of glassy carbon electrode (GCE) for BIA-amperometry of INZ (Quintino and Angnes, 2006), DPV at HMDE for simultaneous determination of INZ and RIF (Leandro et al., 2009), use of dropping mercury electrode (DME) for simultaneous determination of INZ and RIF by differential pulse polarography (DPP) combined with support vector regression (SVR) (Asadpour-Zeynali and Soheili-Azad, 2010) and renewable pencil graphite electrode (PGE) for detection of RIF by differential pulse adsorptive stripping voltammetry (DPASV) (Kawde et al.,

Table 1
Some of non-sensor based methodologies reported for the determination of INZ and RIF.

Method	Analyte(s)	Sample	LOD (μg ml^{-1})	LOQ (μg ml^{-1})	References
Fluorimetry	INZ	Tablets	0.0343	NR	Lapa et al. (2000)
HPLC/UV	RIF and related compounds	Tablets	0.2	1	Liu et al. (2008)
	PZM	Plasma	PZM: 0.014	PZM: 0.1	Zhou et al. (2010)
	AcINZ		AcINZ: 0.009	AcINZ: 0.05	
	INZ		INZ: 0.023	INZ: 0.1	
	RIF		RIF: 0.054	RIF: 0.2	
	PZM	FDC Tablets	PZM: 0.13	PZM: 0.40	Wang et al. (2012)
	INZ		INZ: 0.08	INZ: 0.24	
	RIF		RIF: 0.20	RIF: 0.60	
	EBH		EMB: 0.10	EMB: 0.30	
	RIF	Synthetic mixture: RIF, OFX and PLGA polymer	RIF: 0.0921	RIF: 0.2790	Shah et al. (2019)
	OFX		OFX: 0.0914	OFX: 0.2771	
RP-HPTLC/UV	PZM	FDC Tablets	NR	NR	Shewiyo et al. (2012)
	INZ				
	RIF				
	EBH				
RP-HPLC/UV	INZ	Plasma	INZ: 0.6	INZ: 1.8	Prasanthi et al. (2015)
	RIF		RIF: 0.13	RIF: 0.4	
	PZM		PZM: 0.5	PZM: 1.6	
MLC	INZ	Urine	0.01	0.03	Mishra et al. (2018)
CFCL-ANNC	INZ	Tablets	INZ: 0.03	NR	Li et al. (2005)
	RIF		RIF: 0.005		
GC	INZ	Serum	1.25	NR	Khuhawar and Zardari (2006)
	HZN				
HPLC-ANN	RIF	Tablets	RIF: 0.133	RIF: 0.200	Glass et al. (2007)
	INZ		INZ: 0.111	INZ: 0.150	
	PZM		PZM: 0.137	PZM: 0.150	
CZE/UV	PZM	FDC Tablets	NR	INZ: 2.50	Faria et al. (2010)
	INZ			RIF: 2.09	
	RIF			PZM: 4.79	
	EBH			ETB: 9.65	
FI-CL	INZ	Tablets	0.0027	NR	Song et al. (2017)
UV–Vis	INZ	Tablets	With EPI: 1.500 With HPC: 5.150	With EPI: 4.545 With HPC: 15.620	Shetty et al. (2012)
Multivariate visible spectrophotometry	RIF	Urine	RIF: 60	RIF: 190	Stets et al. (2013)
	INZ		INZ: 40	INZ: 130	
UV	RIF	FDC Tablets	RIF: 1.653	RIF: 5.007	(Arifa Begum et al., 2013)
	INZ		INZ: 0.585	INZ: 1.772	
HILIC-MS/MS	PZM	Plasma	NR	PZM, RIF and INZ: 0.004	Zhou et al. (2013)
	RIF			EMB: 0.0005	
	INZ			STM: 0.01	
	ETB				
	STM				
Spectrophotometry	INZ	Tablet	0.98	NR	Zargar et al. (2013)
LC–MS/MS	RIF	DBS	NR	RIF: 0.15	Vu et al. (2014)
	CLR			CLR: 0.05	
Titrimetry	INZ	Tablet	NR	NR	Swamy et al. (2015)
UV	RIF	Urine	Method A (263 nm): 0.19 Method B (259 nm): 0.14	Method A: 0.57 Method B: 0.44	Swamy et al. (2018)
Colorimetry	INZ	Saliva	1.25	NR	Korrapati et al. (2017)

Abbreviations: **RIF**: rifampicin, **PZM**: pyrazinamide, **INZ**: isoniazid, **AcINZ**: acetyl isoniazid, **FDC:** fixed dose combination, **EBH**: ethambutol hydrochloride, **ETB**: ethambutol, **HZN**: hydrazine, **STM**: streptomycin, **CLR**: clarithromycin, **PDXH**: pyridoxine hydrochloride**, HPLC:** high performance liquid chromatography**, UV:** ultraviolet spectrophotometry, **FDC:** fixed dose combination, **PLGA**: poly (lactic-co-glycolic acid), **RP-HPTLC:** reversed-phase-high performance thin layer chromatography, **RP-HPLC:** reversed phase-high-performance liquid chromatography**, MLC**: micellar liquid chromatography**, CFCL-ANNC:** continuous-flow chemiluminescence with artificial neural network calibration**, ANN:** artificial neural network**, CZE**: capillary zone electrophoresis, **FI-CL**: flow injection chemiluminescence, **UV–Vis**: ultraviolet–visible spectrophotometry, **EPI:** epichlorohydrin, **HPC:** 4-hydroxyphenacylchloride, **HILIC-MS/MS:** hydrophilic interaction chromatography coupled with tandem mass, **LC–MS/MS:** Liquid chromatography tandem mass spectrometry, **DBS:** dried blood spots.

2014).

Investigations at bare electrodes, generally present large overpotential (more than 900 mV at bare GCE for example (Lima et al., 2016)) and low sensitivity for the oxidation of INZ due to sluggish electron transfer kinetics (Zare et al., 2009; Cheemalapati et al., 2014a, b). In addition, many of the above mentioned sensors have been operated in excessive pH conditions and/or fabricated by elements that can easily contaminate the environment (Yun Xia and Ya Hu, 2005). The toxicity of mercury also limits the application of these kinds of electrode out of laboratory. Some solutions have been presented to address this problem. For instance, renewable silver amalgam film electrode can be an alternative for HMDE and DME (Szlósarczyk et al., 2012). Cyclic renewable mercury film silver based electrode (Hg/AgFE) was first described by Baś and Kowalski, (2002) and then successfully used for the determination of several metal ions such as chromium (Baś, 2006), manganese (Piech et al., 2008), molybdenum (Piech, 2008), selenium (Piech, 2008), uranium (Piech et al., 2007) and gallium (Piech, 2011). DPV determination of INZ using Hg/AgFE was reported by Szlósarczyk and coworkers in 2012 with nanomolar limit of detection (LOD) and quantification (LOQ) and good precision (Szlósarczyk et al., 2012).

The use of mediators to catalyze the analyte oxidation is an inexpensive and simple way to improve the response at bare electrodes.

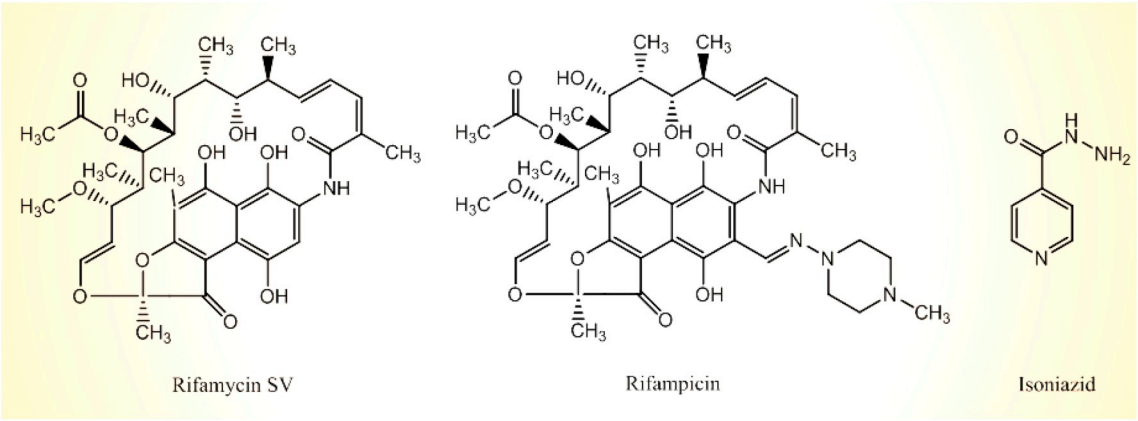

Fig. 1. Structures of rifamycin SV, rifampicin and isoniazid.

Ferrocenyl derivative, (FcM)TMA, as homogeneous mediator has been shown to catalyze the oxidation of INZ at the bare platinum electrode drastically (with catalytic rate constant of $3.98 \pm 0.10 \times 103\ M^{-1}s^{-1}$). This catalyst is stable in different supporting electrolyte solutions (Gao et al., 2006). 1,2-dihydroxyanthraquinone-3-sulfonic acid disodium salt (Alizarin Red S or ARS) is another mediator which has been effectively employed for electrochemical sensing of INZ at unmodified GCE (Karimi et al., 2010). The maximum peak current was observed in pH 6 and in ARS concentration of 100 mmol L^{-1}. The method presented very good selectivity in the presence of high concentrations of potential interferents.

4.2. Electrode modifiers in electrochemical sensing and biosensing platforms

An effective common approach to overcome the high overpotential and electrode fouling as well as to enhance analyte adsorption, electrochemical response and selectivity is the modification of working electrode with an appropriate electrocatalyst accommodated modifier (Tyszczuk and Korolczuk, 2009; Azad et al., 2015). Electrode modifiers must be compatible with the chosen electrocatalyst as well as the target molecules and have little fouling properties. To minimize the fouling effect, electrode materials and electrolyte should be selected carefully. Several techniques have been utilized for fabrication and characterization of modifier film on the surface of electrodes. Modifications usually accomplish by drop casting, electrodeposition, and electropolymerization methods.

Several electrochemical, morphological and structural characterization methods are commonly used for studying the modifiers including cyclic voltammetry, electrochemical impedance spectroscopy (EIS), electron microscopy, atomic force microscopy (AFM), X–ray photoelectron spectroscopy (XPS), energy-dispersive X-ray spectroscopy (EDS or EDX), Fourier-transform infrared (FT-IR) spectroscopy, Raman spectroscopy (RS), thermogravimetric analysis (TGA), etc. In the following parts, we tried to describe nearly all types of modifications that have been worked to date in electrochemical quantification of INZ and RIF.

4.2.1. Surfactants modifiers

Surfactants have been shown to have some advantages for modifications of different electrodes including decrease of the resistance at concentrations higher than critical micellar concentration (CMC) (Albahadily and Mottola, 1987) and increase of response and selectivity (Gutiérrez-Fernández et al. 2004).

Cationic (cetyltrimethylammonium chloride or CTAC) and anionic (sodium dodecyl sulfate or SDS) surfactants were investigated for in situ modification of CPE at concentrations lower than CMC. These modified electrodes were compared with unmodified CPE in determination of RIF and rifamycin SV (Fig. 1) in acidic pH condition. SDS-modified CPE enhanced the current and selectivity in adsorptive voltammetry of RIF while CTAC modification led to selective determination of rifamycin SV in the presence of RIF (Gutiérrez-Fernández et al. 2004). The next study was carried out by Atta's team for electro-oxidation of INZ. They examined three anionic, three cationic and two nonionic surface-active agents for in situ modification of CPE. All the explored cationic and nonionic surfactants where shown to decrease oxidation current signal except SDS and sodium dodecyl benzene sulfonate (SDBS) which have been shown to increase the signal (Atta et al., 2011a,b). In the end of 4.2.2 and 4.2.4 we point out two other uses of surfactant in modified electrodes.

4.2.2. Polymeric modifiers

The first polymer coated electrode in the area was introduced in 2004 by Girousi's group for the determination of RIF. Their DNA-sensor showed brilliant LOD (8×10^{-15} M) in comparison to bare CPE (0.25×10^{-7} M) (Girousi et al., 2004). Afterward, several organic and inorganic polymers have been used unaccompanied or in conjunction with other components.

Polypyrrole (OPPy), is an appropriate material for sensing applications. Its overoxidized form (OPPy) is a conducting cation permselective polymer, with anti-fouling and anti-interfering properties (Palmisano et al., 1995; Majidi et al., 2006). Majidi's team, successfully applied OPPy-modified GCE for simultaneous CV-based determination of INZ and HZN. Multivariate methods were coupled with voltammetry to solve the problem associated with oxidation peaks overlap of INZ and HZN (Majidi et al., 2005). In their next effort, they used the sensor for electro-oxidation and amperometric determination of INZ which led to large decrease in overpotential (345 mV) in a wide range of pH (Majidi et al., 2006).

An amperometric sensor for RIF analysis was prepared by immobilization of beta cyclodextrin on the surface of the platinum electrode using electro-polymerization of OPPy (Lomillo et al., 2005). The obtained values for repeatability and reproducibility of the sensor was found to be 2.28% and 3.51% respectively. The selectivity of the method is unclear, because of insufficient interference tests.

Some poly amino acids have also been reported for electrode modifications such as histidine (His) and tyrosine (Tyr). Earlier studies showed that Screen-printed carbon electrode (SPCE) can be coated by poly-L-His (PLH) for the determination of ascorbic acid (AA) (YU et al., 1996) and chromium(VI) (Bergamini et al., 2007). PLH in complex with copper(II) has also been applied for biosensing of L-ascorbate (Hasebe et al., 1998). Bergamini' team in 2010 used PLH-modified SPCE for the determination of INZ in urine samples (Bergamini et al., 2010). Despite the disposability of SPCE, the usability of device was found to be more than 50 times. Cheemalapati's research team successfully tested

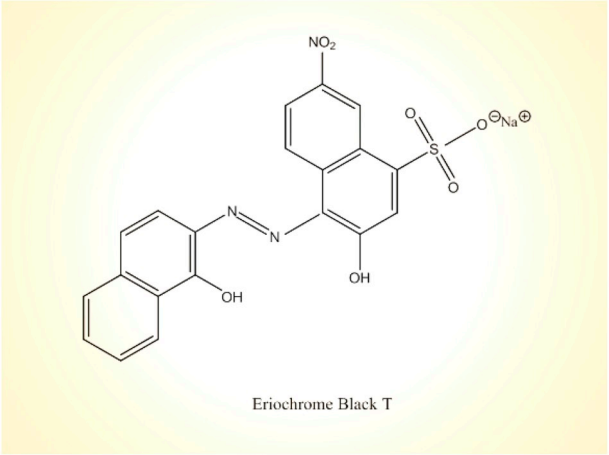

Fig. 2. Structure of Eriochrome black T.

electro-polymerized Tyrosine-modified GCE for the determination of four drugs (an anti-hypertension drug, hydralazine hydrochloride (HDH) and also three anti-tubercular agents, INZ, PZM and ethambutol hydrochloride (EBH)) (Cheemalapati et al., 2014a,b). The modified electrode presented relatively high LOD but appropriate repeatability and reproducibility (RSD less than 3%).

CV assisted electro-polymerized polyamido sulfonic acid (PASA) has been investigated for GCE surface modification aimed at INZ determination (Yang et al., 2008). Acceptable results were obtained in analysis of pharmaceutical formulations with this electrode. However, the device was not tested for analysis of human body fluid specimens.

Nafion® (Nf), copolymer of perfluorinated vinyl ether and tetrafluoroethylene (TFE), is the first synthetic ionomer (ion containing polymer) which was discovered in 1960s. Nf is a strong cation exchanger and a very powerful acid catalyst with great chemical, mechanical and thermal stability. Nf have been frequently applied as membrane in fuel cell and electrolysis of sodium chloride solutions despite the development of its nonfluorinated counterparts. Nf has also been used in solar energy, batteries, photocatalysis and electrode modification (Heitner-Wirguin, 1996; Mauritz and Moore, 2004; Lu et al., 2010). Azad and Ganesan used an inorganic metal complex for successful oxidation and sensitive amperometric quantification of INZ. Sulfonate head group of Nf, were utilized to immobilize Fe $(tmphen)_3^{2+}$ on the surface of Nf coated GCE. This modified electrode was efficiently able to electrocatalize the oxidation of INZ in 0.1 M Na_2SO_4 with 240 mV decrease in overpotential (Azad and Ganesan, 2012). Only 6% of the initial signal was lost after 50 times analysis of INZ. Slow diffusion of INZ and consequently low sensitivity (0.0025 μA μM^{-1}) and high LOD (13 μM) were of disadvantages of the sensor. Furthermore, no human sample examination was performed with the device.

Another extensively studied conducting polymer is Poly (3,4-ethylenedioxythiophene) or PEDOT which has been employed thus far for the determination of several compounds such as dopamine (DA) (Kumar et al., 2005) and morphine (Ho et al., 2005). Electrochemical behavior of INZ at PEDOT-modified platinum electrode in the presence of anionic (SDS) and cationic (CTAB) surfactants was investigated using CV, LSV and EIS. PEDOT/PtE was then applied for the purpose of INZ in pharmaceutical and biological (human urine) samples. In the presence of SDS or in the absence of CTAB, negative shift of peak potential was observed by rise of pH, perhaps because of more facile deprotonation. Further adsorption of INZ, lower charge transfer resistance and higher current response was observed with SDS in pH 2.3 and with CTAB in pH $\geq$ 7.4. Negatively charged SDS film led to faster diffusion of INZ towards the PEDOT/PtE, electrostatic repulsion of anionic interferents (like AA and UA) at pH 2.3 and therefore enhanced selectivity (Atta et al., 2011a,b).

Eriochrome black T (EBT) (Fig. 2), is a water-soluble indicator commonly used in complexometric titration. Poly EBT (PEBT)-modified electrodes has been used for voltammetric determination of various biomolecules such as DA (Chandra et al., 2010) and epinephrine (Yao et al., 2007). In two different investigations, Asadpour-Zeynali and his coworker, utilized electrocatalytic activity of PEBT for oxidation and determination of INZ on the surface of GCE (Asadpour-Zeynali and Arteshi, 2017) and Pencil Lead Electrode (PLE) (Asadpour-Zeynali and Arteshi, 2017). Unfortunately, relatively poor LOD was obtained in both mechanisms in comparison to other reported electrodes.

4.2.3. Metal films and metal-based nanomaterials

Lead film electrodes has been applied for electroanalysis of inorganic (Korolczuk et al., 2005; Korolczuk and Tyszczuk, 2006) and organic (Korolczuk and Tyszczuk, 2007; Tyszczuk, 2008) analytes with LODs lower than those obtained by bismuth film electrode. In a study in 2009, lead film electrode was employed for AdSV analysis of pharmaceutical formulations of RIF in pH 5 with low LOD and good selectivity (Tyszczuk and Korolczuk, 2009). These types of electrodes have several advantages. They are much safer than mercury electrodes, provide fast measurements, can be easily regenerated (Tyszczuk and Korolczuk, 2009) and are appropriate for use in flow systems (Korolczuk et al., 2005). In the same year, dysprosium hydroxide nanowires (DyNW)-modified CPE was prepared by Daneshgar's research group for square-wave adsorptive stripping voltammetry (SWAdSV)-based determination of RIF in commercial capsules and spiked human urine samples. Their nano-sensor exhibited recovery value of 99.9% with RSD value of 0.04 for 7 replicate determinations and sub-nanomolar limit of detection and quantification (Daneshgar et al., 2009).

Clays are stable layered nanostructures of hydrated aluminum silicate minerals with ion exchange capability which has been frequently used as electrode modifier for sensing applications (Mousty, 2004). Fe $(dmbpy)_3^{2+}$ (where dmbpy is 4,4′-dimethyl-2,2′-bipyridine) was immobilized as electrocatalyst on bentonite clay films. The films showed stable, reproducible redox current after few initial scans and proficient catalytic activity towards the electro-oxidation of INZ (more than 150 mV decrease in overpotential). This property was consequently utilized to construct an electrochemical sensor for INZ determination in pharmaceutical samples. Presence of RIF didn't alter the oxidation current in the determination (Azad et al., 2015), but nitrite or arsenite, might interfere with the analysis.

Metal nanoparticles electrode modifiers have attracted considerable attentions in last decade owing to excellent catalytic activity. INZ determination by linear sweep voltammetry (LSV) was reported by Cheemalapatia's group using GCE electrochemically modified with 40–300 nm rhodium nanoparticles (RhNPs) (Cheemalapati et al., 2014a, b). Despite neutral condition workability, good selectivity, repeatability and reproducibility, the nanosensor displayed relatively high LOD and low sensitivity (perhaps because of large diameter of particle).

Jena and Raj, for the first time, employed gold nano-particles (AuNPs) decorated sol-gel based electrodes for simultaneous amperometric determination of INZ and HZN (Jena and Raj, 2010). To make a stable platform, in the first step, polycrystalline gold electrode (PCGE) was modified by a 3D silicate network. Aftewards, colloidal AuNPs with 70–100 nm diameter added to the network using a process called "seeding" (Brown and Natan, 1998) which utilize NH_2OH/Au^{3+} solution and hydroxylamine for enlargement of colloidal AuNPs. The modification decreased the oxidation overpotential of INZ by 450 mV in comparison to PCGE and showed excellent sensitivity (4.03 ± 0.01 μA μM^{-1}). However, no interference experiment was performed in their investigations to determine the selectivity of the nano-sensor.

A palladium-modified carbon ionic liquid electrode (CILE) was made by Absalan and his coworkers through electrodeposition of 30–100 nm palladium nanoparticles (PdNPs) on the surface of CILE (Absalan et al., 2016). The electrochemical response signal of INZ was greatly improved and overpotential, was also decreased remarkably (280 mV) due to

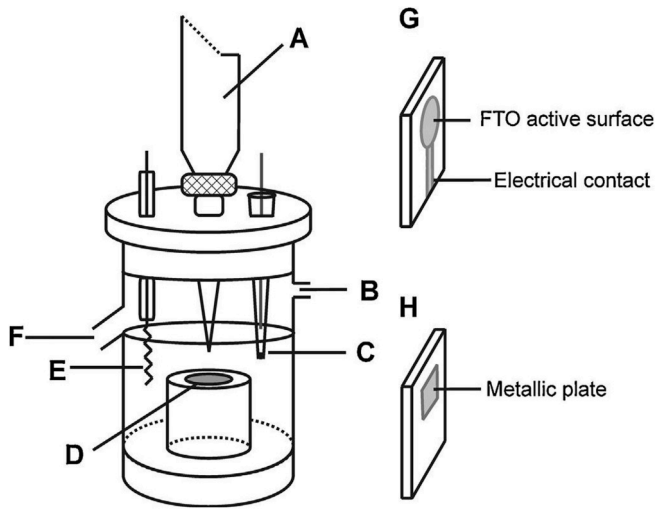

Fig. 3. Schematic illustration of the batch injection cell adapted to FTO electrodes comprising (A) motorized micropipette; (B) output for electrical contactwire; (C) reference electrode; (D) circular magnetic plate over cylindrical platform; (E) auxiliary electrode; and (F) cell drain. (G) Front and (H) back views of the FTO electrode. Reprinted with permission from Ref (Martins et al., 2014).

synergistic effect of CILE as substrate and good properties of PdNPs. INZ showed a well-defined oxidation peak with high current at the modified electrode. The stability of the sensor was also great. Its initial response was decreased by only 5% after 40 days storing in the air.

Perhaps due to instability of chemical modifications of electrodes under strong hydrodynamic state of flow injection analysis (FIA) (Bergamini et al., 2010; Azad et al., 2015; Lima et al., 2016), the reports for FIA-based electrochemical quantification of INZ are rare (Shah and Stewart, 1983; Nellaiappan and Kumar 2017). Oliveira's research group used silver hexacyanoferrate nanoparticles (AgHCFNPs)-modified SPCE to construct a disposable FIA-based sensor for amperometric determination of INZ. A tiny flow cell with effective volume of 95 µl was designed for measurements. The sensor presented good accuracy and precision, high sample frequency (24 injection h^{-1}) and usability (more than 100 experiments) (de Oliveira et al., 2012).

Batch injection analysis (BIA) is a high producible analytical system with low reagent consumption and high sample frequency which was first introduced by Wang and Taha, (1991). In comparison to FIA, BIA doesn't show carryover effect and is portable, because the use of BIA cell and micropipette has eliminated the pumps, valves, tubes, and electrolyte reservoir. (Wang and Taha, 1991; Quintino and Angnes, 2004a,b). BIA is less suitable for long-lasting reactions as the injector is adjacent to the detector. However, it theoretically can be more suitable for biocatalytic sensors and modified electrodes. Due to the wall-jet principle of BIA, sample zone created above the surface of detector can't be affected by surrounding solution (Wang, 1992). BIA associated with amperometry (BIA-AMP) is a powerful technique which has been frequently used in sensing platforms due to providing unique sharp transient signal of current (Quintino et al., 2002; Quintino and Angnes, 2004a,b; Ferreira et al., 2012). High throughput (about 400 h^{-1}) BIA-AMP analysis of INZ was performed for the first time using fluorine-doped tin oxide (FTO) electrodes modified by nickel hydroxide ($Ni(OH)_2$), cobalt hydroxide ($Co(OH)_2$) and two types of $NiCo(OH)_2$ nanomaterials with 5–10 nm diameter (Schematic illustration is represented in Fig. 3) (Martins et al., 2014). The best sensitivity was obtained from the $NiCo(OH)_2$ with 75:25 ratio. Since no interference study was done by the researchers, the selectivity of the proposed method is unidentified.

Bismuth oxide ($Bi_2O_{2.33}$) nanorods (50 nm × 300–400 nm) were prepared for modification of screen-printed electrode (SPE) through drop-casting procedure to fabricate a sensitive sensor for simultaneous detection of INZ and AC. The nano-sensor was successfully applied for the determination of these drugs in pharmaceutical tablets and also three human body fluids (serum, urine and saliva) (Mahmoud et al., 2017). The modified electrode presented excellent precision (RSD values for five repetitive measurements of AC and INZ was calculated to be 0.27% and 0.08% respectively) and reproducibility (RSD values for three distinctly fabricated electrodes was found to be 1.7% and 2.1% for AC and INZ respectively). But the optimum pH for the determination was very harsh (pH 2) and in higher pH values, the oxidation peaks of INZ and AC interfered with together.

LDHs with formula of $[M^{II}_{1-x}M^{III}_{x}(OH)_2]^{x+}\ A^{n-}_{x/n}mH_2O$ are nontoxic positively charged lamellar nanomaterials. M^{II} and M^{III} signify divalent and trivalent metals respectively, $x = M^{III}/(M^{II} + M^{III})$ and A^{n-} is interlayer anionic group (Alexa et al., 2011). LDHs have been exploited in many technical areas owing to high stability, anion exchange capability and their adsorptive and catalytic properties. Asadpour-Zeynali and colleagues electrodeposited Fe/Al–NO_3-LDH film on the surface of GCE by chronoamperometry for electrocatalytic reduction and quantification of INZ (Asadpour-Zeynali et al., 2016). This was one of the rare reports on the electrocatalytic reduction (in contrast to electrocatalytic oxidation) of INZ. In their study however, no repeatability, reproducibility, stability and interference studies were accomplished.

Nickel nanoparticles (NiNPs) has also been used in drug sensing. In NiNPs-based electrochemical sensors, catalytic oxidation of the analyte takes place just in very high pH condition which can be detriment for sensitive species (Neiva et al., 2014; Neiva et al., 2016). Nickel hexacyanoferrate (NiHCF) as a redox mediator may be a good substitute. In recent study by Oliveira and his colleagues, GCE was modified with a thin layer of irregular shaped NiHCF nanoparticles (~40 nm) and then tested for voltammetric determination of RIF (de Oliveira et al., 2018). The selectivity of this sensor, however, was not determined and similar to NiNPs-based nanosensor, the analysis in this work was taken in an extreme pH condition (pH 3). In their next work, Oliveira's group reported the use of copper hexacyanoferrate nanoparticles (CuHCFNPs) for fabrication of amperometric INZ sensing device (Oliveira et al., 2018). For that, biochar-modified CPE (BM/CPE) was electrochemically decorated with 305 ± 42 nm CuHCFNPs. The modification heightened the sensitivity of the sensor by ~4 folds. The sensor was found to be susceptible to interference of high concentration (1.0×10^{-4} M) of RIF and AA. Nevertheless, it is not problematic, because un-metabolized form of this molecules does not surpass this concentration.

For the first time, potentiometric electroanalysis of INZ was reported by Shabani and his associates. Their nanobiosensor comprised of iron oxide magnetic nanoparticles (Fe_3O_4MNPs)-modified CPE and showed excellent LOD (3.09×10^{-13} M) (Shabani et al., 2018).

4.2.4. Carbon based nano-modifiers

Carbon nanomaterials (graphene oxide (GO), reduced graphene oxide (RGO), carbon nano fibers (CNFs), carbon nanotubes (CNTs), ordered mesoporous carbon (OMC), etc.) have been broadly used in electroanalysis, alone or in combination with other modifiers (Ratinac et al., 2011). In the following parts, we first briefly describe the useful characteristics of each material and then bring up their recent sensing employments for INZ and RIF determination.

4.2.4.1. Reduced graphene oxide (RGO). Graphene oxide (GO), is a honeycomb nanostructure with mostly sp^2-and some sp^3-hybridized carbon atoms and abundant functional groups (Ratinac et al., 2011). GO has drawn great considerations owing to its large surface area, strong mechanical strength and high hydrophilicity (Cheemalapati et al., 2013). However, GO-based materials usually have relatively low conductivity and catalytic activity. Instead, reduced GO (RGO) has high electrical conductivity and large surface area (larger than that of carbon nanotubes) (Yao et al., 2012; Yao et al., 2013; Du et al., 2014; Ren et al., 2014) and has been widely used for designing different modified

electrodes in electrochemical sensors. In chemical and thermal reduction, use of carcinogenic and/or toxic chemicals (like hydrazine hydrate (Stankovich et al., 2007), hydroxylamine (Zhou et al., 2011) and hydroquinone (Wang et al., 2008)) or high temperature is usually needed respectively which can potentially result in toxicity and/or formation of contaminating species or degradation of components (Hernandez et al., 2008). Electrochemical approaches, instead, are simple, green and fast methods for preparation of RGO (Guo et al., 2009). Electrochemically reduced (electro-reduced) graphene oxide (ERGO) has been recurrently applied in sensing studies (Palanisamy et al., 2012). The first electrochemical determination of INZ based on the ERGO was reported by Cheemalapati and coworkers (Cheemalapati et al., 2013). Unfortunately, no biological specimen analysis and interference experiment was done in their work and moreover, their device suffered from relatively low stability (6% loss of initial signal in less than 1 day).

Gallic acid or GA is a naturally occurring organic acid with formula of $C_6H_2(OH)_3COOH$. GA exhibits reducible properties due to OH and COOH functional groups in its benzene ring. For the first time, Jing Li's team used gallic acid reduction process as a green method for preparation of RGO (Cao et al., 2016). Recently, GA induced RGO was applied to modify GCE for amperometric determination of INZ (Balasubramanian et al., 2017). The device presented long term stability (only 1.3% decrease of current response after 3 weeks), satisfactory reproducibility (RSD value of 3.2% for 5 independently fabricated modified electrodes) and high selectivity in interference experiments with 50-fold excess concentrations of 5 different interferents (DA, UA, AA, Glucose and Sucrose).

High electrical conductivity and surface area of RGO can increase the background currents so that the determination of trace analyte quantities becomes challenging (Güell et al., 2010). Additionally, reduction process may reduce the electrocatalytic activity, sensitivity and stability (Lim et al., 2010; Zhang and Yin, 2014). Accordingly, GO with lower oxygen content (partially reduced GO) can be a valuable nanomaterial. Partial electro-reduction of GO make it possible to optimize the balance between conductivity and electron-transfer action capacity (proper number of functional oxygen groups) (Rastgar and Shahrokhian, 2014). Zhu's group synthesized different extents of ERGO films for electroanalysis of INZ under the control of CV. According to the cycle number of CVs (1, 3, 5, 7, 9, 11, 13, 15) applied for electrochemical reduction of GO, partially reduced ERGOs (pERGOs) with different degrees of reduction were formed. GCE coated with ERGO5 showed the maximum current response towards the oxidation of INZ and presented low background, good selectivity, anti-fouling activity and acceptable stability (6% decrease in response value after 15 days measurement) (Zhu et al., 2015).

4.2.4.2. Multi-walled carbon nanotubes (MWCNTs). Thanks to their particular structure, electrical and electrocatalytic characteristics, CNTs have been increasingly employed in many areas including analytical chemistry (Ajayan, 1993; Merkoçi, 2006) and fabrication of fast responsive sensitive sensors (Wang, 2005). Edge-plane-like graphite sites at the CNTs ends give them particular electrocatalytic activity which can be improved by further functionalization. The large available active surface of CNTs resulted from their special geometry (Rivas et al., 2007; Agüí et al., 2008), can be exploited in electrode modification to augment the analytical performances through increasing the faraday currents as well as decrease of background charging current (Rubianes and Rivas, 2003; Antiochia et al., 2004; Shahrokhian and Amiri, 2007), response time, electrode fouling and overpotential (Ghica et al., 2009; Murugesan et al., 2011).

Shahrokhian's group fabricated a renewable sensor using MWCNTs. Electrochemical behavior of INZ on the multi-walled carbon nanotube paste electrode (MWCPE) was compared with the one on the surface of unmodified conventional CPEs using cyclic voltammetry in pH 4. The modified electrode then was applied for the determination of INZ by the DPV. Modification with MWCNTs resulted in decreased background current and overpotential (151 mV decrease in overpotential), significant improvement in peak currents and also superior selectivity (more than 450 mV differences in Epa of sulfhydryl containing interferents in DPV voltammograms) (Shahrokhian and Amiri, 2007). Shahrokhian's team, further modified the electrode by thionine immobilization for the simultaneous determination of AA, acetaminophen (AC) and INZ which led to negative shifts in anodic peak potentials and high resolution (Shahrokhian and Asadian, 2010). Different amounts of thionine immobilized MWCNT (T-MWCNT) was incorporated in the matrix of CPE (5%, 15% and 20% W/W) to select the finest one. The superlative results were obtained from 15% (W/W) T-MWCNT based on CV and DPV experiments on 0.1 mM AA and AC. Further addition of T-MWCNTs led to increase in background current, decrease in the anodic peak currents and worsen peak separation. Acceptable stability (just 3.2% decrease in peak current after 2 weeks keeping in air) and recovery (97.3–102.6%) was obtained by T-MWCNT-modified electrode. Nevertheless, acidic (pH 4) operational condition and insufficient interference experiments were of weaknesses of their work.

Aimed at INZ determination, functionalized MWCNT (f-MWCNT) was prepared by ultrasonication of purified MWCNT in acid solution to modify GCE (Chen et al., 2012). Negative groups of f-MWCNTs led to faster oxidation reaction through easy diffusion of INZ to the surface of GCE. In comparison to bare GCE and other employed electrode modifiers (MWCNT, GO and RGO), f-MWCNT showed the maximum peak current (about 7 times higher than MWCNT) and 400 mV decrease in overpotential (Chen et al., 2012).

Approaches have been applied for CNTs immobilization on electrochemical transducers include dispersion in different solvents or incorporation in composite matrices using distinct binder (Li et al., 2006; Kim et al., 2012; Salimi et al., 2013). Some biopolymers like chitosan (chit) has been exploited as matrices in combination with other modifiers. Chitosan, a linear b-1,4-linked polysaccharide (similar to cellulose) is the structural component of the exoskeleton of crustaceans and the cell walls of fungi that can be obtained by the partial deacetylation of chitin (Phillips and Williams, 2009). It possesses many advantages, such as excellent strong film forming ability with high water permeability, good adhesion and high mechanical strength. In an investigation by Satyanarayana and coworkers, a stable composite film of chitosan (as dispersant) and f-MWCNT was made-up on the surface of GCE to make a powerful electrochemical nano-sensor for the determination of INZ (Satyanarayana et al., 2014). SEM images revealed the homogenous porous architecture of f-MWCNT/chitosan nanocomposite film. The modifier remarkably enhanced the voltammetric signal response and greatly lowered the oxidation overpotential of INZ (about 800 mV). The described modified electrode could be used for the detection of ppb levels (LOD = 7.5 ng mL^{-1}) of INZ with high selectivity in the presence of biological interferents. RSD values for repeatability and reproducibility were determined to be 2.5% and 2.2% respectively.

MWCNT has also been used in combination with CTAB (Buddanavar et al., 2016). The modification of GCE with MWCNT and CTAB led to enhancement of the active surface area of the electrode by 3 fold (0.128 cm^2 in comparison to 0.0397 cm^2). The electrode was then subjected to INZ determination in human urine and plasma. Exhaustive interferents experiments revealed that the sensor possessed high level of selectivity.

4.2.4.3. Ordered mesoporous carbon (OMC). OMC is another advanced carbon material with additional useful features such as adjustable regular porous architecture, and anti-fouling activity (Ryoo et al., 1999). Since its discovery (in 1999), OMC has been recurrently used as electrode modifier in electrochemical sensing of different analytes (Hu et al., 2009; Zheng et al., 2009; Zhang et al., 2014). For the first time, Nf-OMC-modified GCE was employed for amperometric determination of INZ in neutral condition and resulted in a large decrease in over-potential and improved electrochemical response (Ratinac et al.,

2011). However, determinations were only performed in pharmaceutical preparations rather than biological fluids. In addition, measurements were found to be affected a little by 4-acetamidophenol in interference study.

4.2.5. Multifarious nanocomposites modifiers

Especially in the last three years, a growing interest has been arisen toward the fabrication of mixed nanocomposite matrices for nano-sensing and nano-biosensing of INZ and RIF due to their synergistic effects on electrochemical and mechanical performance of devices. Nanocomposite based sensory arrays can be useful to maximize the selectivity and resolution, especially when multi-analyte detection of close species is desirable.

4.2.5.1. Nanocomposites of graphene derivatives and polymers. Cysteic acid (CA) can be obtained from electrochemical oxidation/polymerization of L-Cysteine (Zhang et al., 2013a,b). Several CA-modified electrodes have been exploited for electroanalysis of drugs including DA (Wang et al., 2007) and TP (Brunetti and Desimoni, 2009). Investigation with GCE modified with CA/GR nanocomposite showed significantly higher oxidation peak current of INZ than that of unmodified electrode (Si et al., 2015). Detailed interference studies (with uric acid (UA), AA, DA, three different salts, two sugars and five amino acids) revealed that the modified electrode possess high level of selectivity. The down side of the device, however, was acidic condition requirement for operation. L-arginine is another amino acid which used in polymeric form for INZ determination. Poly-L-arginine (PLA) is able to electrostatically interact with negatively charged groups of GO (Zhang et al., 2013a,b). Cheemalapati's group, fabricated a PLA/GO nanocomposite-modified GCE for simultaneous DPV -based determination of buspirone hydrochloride (BPH), INZ and PZM in pH 7 (Devadas et al., 2015). Their device was then successfully employed in quantification of the target analytes in commercially available tablets as well as real samples (human blood serum).

The normal range of UA (2,6,8-trihydroxypurine) in urine is 1.49→4.46 mM (Zhang et al., 2004). Due to closeness of the oxidation peak potentials of INZ and UA (0.58 V and 0.47 V respectively) (Lin and Jin, 2005; Yang et al., 2008), and therefore overlapping in the oxidation signals, detecting INZ in the presence of high concentrations of UA (urine and plasma) can be problematic. Accordingly, developing reliable method for accurate and simultaneous detection of these two analytes is of great clinical significance.

Yana and colleagues, designed a Poly (sulfosalicylic acid) (PSA)/electro-reduced carboxylated graphene (ERCGO)-modified GCE (PSA/ERCGO/GCE) for simultaneous analysis of INZ and UA in urine samples in alkaline media (Yan et al., 2015). PSA/ERCGO film is charged negatively at pH 9.0 owing to remained anionic carboxyl groups (COO^-) of partial electro-reduced CG as well as abundant anionic sulfonic acid groups (SO_3^-) of PSA. In this condition, INZ and UA showed completely different ionic behaviors, as INZ (pKa = 10.8 (Atta et al., 2011a,b)) is cationic, while UA (pKa = 3.1 (Simic and Jovanovic, 1989) is anionic). Even though the sensor was insensitive to AA (perhaps due to the electrostatic repulsion of AA by the modifier), nonetheless, other potential interferents were not tested to provide better conclusion of its selectivity.

4.2.5.2. Nanocomposites of graphene oxide and metallic (micro/nano) particles. Graphene nano-sheets tend to interact with together. It is possible to overcome this problem through functionalization of graphene with metal nanoparticles (Shao et al., 2010; Tabrizi et al., 2014; Sun et al., 2015). Guo and colleagues, described AuNPs-RGO film coated GCE for electrocatalytic determination of INZ. For preparation of the film, sodium citrate solution was added into ultrasonicated GO/$HAuCl_4$ suspension and after the heat treatment, the final product was utilized for modification of electrode with the concentration of 1.0 mg mL^{-1}. Uniform distribution of AuNPs (10–20 nm) was observed on the entire surface of RGO sheets by electron microscopy. The electrochemical oxidation of INZ with decrease in over-voltage is achieved in neutral media and after three weeks storage, the sensor retained more than 92% of its initial current response (Guo et al., 2015).

In addition to AuNPs, other metallic particles have also been used for decoration of GO-modified GCE. Copper micro particles (CuMPs) were deposited on the surface of GCE pre-modified with GO nanosheets to achieve irregular electrode surface with large surface area (designated as CuMPs/GO/GCE). The system reduced the overpotential (120 mV) and showed anti-interference properties in amperometric detection of INZ in serum and urine samples (Balamurugan et al., 2017).

GCE was also modified with a stable, uniform and thin layer of pERGO/$Ni(OH)_2$NPs nanohybride for LSV-assisted determination of RIF (Rastgar and Shahrokhian, 2014). Microscopic characterization of modifier film discovered even distribution of nickel hydroxide nanoparticles with mean size of 25 nm on the surface of RGO layer. The platform showed satisfactory selectivity and repeatability. However, the stability was not determined.

Recently, Santhanalakshmi and Rajesh, reported SnO_2 nanoparticles (5 ± 0.2 nm)-RGO nanocomposite-modified GCE by simultaneous $SnCl_2$ oxidation and GO reduction. The sensor was applied for electrochemical detection of INZ in pharmaceutical preparations and human urine samples. The device remarkably reduced the overpotential (610 mV) and displayed high stability and low LOD (7 nM) (Santhanalkshmi and Rajesh, 2018). Despite the overall good selectivity, sensitivity to interfering influence of paracetamol was observed in interference analyses.

4.2.5.3. Carbon nanotube-based nanocomposites. MWCNT has also been employed in conjunction with other nanostructures. Researchers fabricated a microfluidic device for amperometric analysis of hydrazine compounds by integration of cobalt hexacyanoferrate (CoHCF) nanoparticle-modified MWCNT/graphite composite electrode (CoHCFNPs/MWCNT/GE) into capillary electrophoresis (Li et al., 2012). Despite the overall good performance, their device displayed very low sensitivity.

A similar sensor was also prepared for INZ determination. The device was comprised of cobalt–iron hybrid hexacyanoferrate nanoparticles (Co-FeHCFNPs) prepared with various proportions on MWCNT coated composite ceramic carbon electrode (CCE). The nanocomposite with Fe^{3+} to Co^{2+} ratio of 1:1 revealed the greatest catalytic activity. The current signal of the analyte was higher on Co-FeHCFNPs/MWCNT/CCE than CoHCFNPs/MWCNT/CCE, Co-FeHCFNPs/CCE and PB/MWCNT/CCE in CV studies. The catalytic activity was also higher in NaCl solutions in comparison to KCl solutions (with the same molar concentration) as supporting electrolyte (Yu et al., 2013). CV-based stability testing disclosed very high stability of the device (less than 2% loss of peak heights following 100 successive cycles).

MWCNT was also utilized for preparation of Gr-f-MWCNT/iron phthalocyanine (FePc) nano composite on the surface of GCE for INZ detection in pH 7.4. More than 200 mV reduction in oxidation potential was achieved using this modifier (Spindola et al., 2017). Gr-f-MWCNT/FePc/GCE and then successfully applied for analysis of saliva and simulated serum specimens.

The more recent use of MWCNT was reported by Huang and associates. They engaged useful electrical attributes of molybdenum carbides (Mo_2C) to make a novel RIF sensory device. To this aim, they heated a mixture of $(NH_4)_6Mo_7O_{24} \bullet 4H_2O$, ethylene glycol and MWCNT at 200 °C for 10 h. After washing and drying, the resulted product (MWCNTs−MoO_2) was converted to MWCNTs−Mo_2C composite by annealing at 800 °C. Prepared composite, then dispersed on the surface of GCE using of chitosan solution. In comparison to MWCNTs/GCE and bare GCE, MWCNTs−Mo_2C/GCE sensor showed much better responses (Zou et al., 2018).

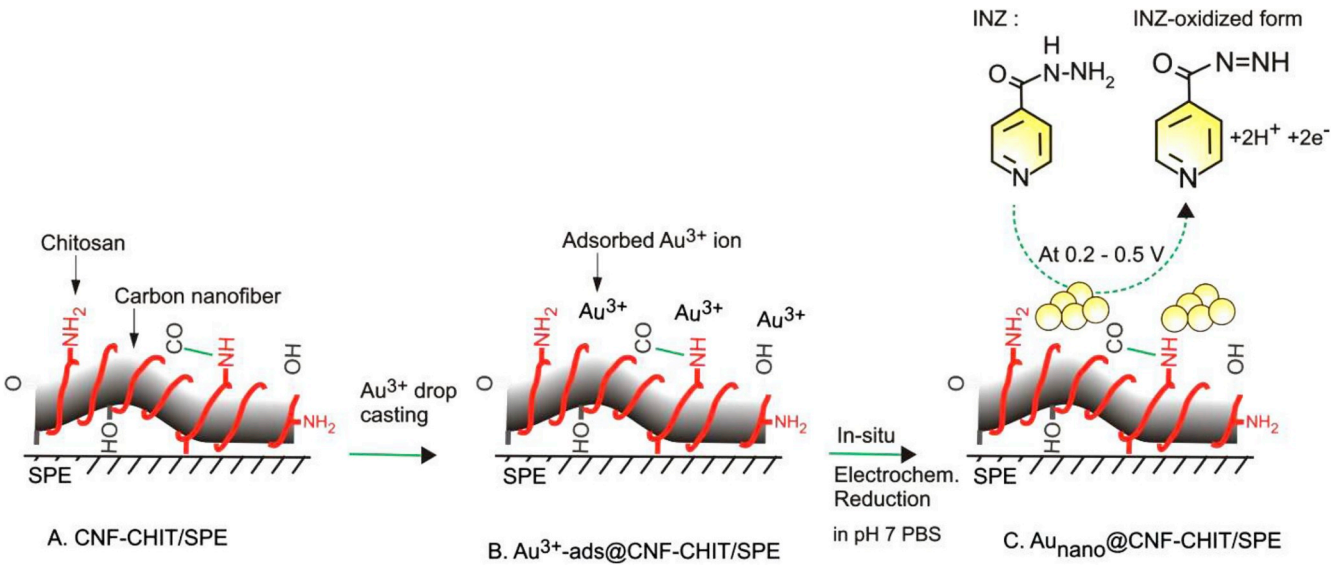

Fig. 4. Preparation and INZ oxidation mechanism of AuNPs@CNF-CHIT/SPE system. Reprinted with permission from Ref. (Nellaiappan and Kumar 2017).

4.2.5.4. Nanocomposites of metallic nanoparticles and conducting polymers. Thanks to their excellent electrocatalytic properties, metal nanoparticles can synergistically improve the characteristics of sensing matrixes especially in combination with advanced polymers (Hüger and Osuch, 2004; Lokesh et al., 2009; Muchindu et al., 2010).

A novel INZ-sensing platform comprised of silver nanoparticles (AgNPs) incorporated in a synthetic copolymer of methyl methacrylate (MMA) and 2-acrylamido-2-methylpropane sulfonic acid (AMPS) (abbreviated as AgNPs/P(MMA-co-AMPS) was designed. Electrochemical appearances of INZ in this device was greatly enhanced owing to interaction of INZ amine group with AgNPs as well as with sulfonic acid group of the copolymer (Rastogi et al., 2016).

Plentiful amine groups of some polymeric modifier such as poly melamine (PMel) lead to decreased aggregation and increased sensitivity (through acting as analyte adsorption sites) which can also be helpful in fabrication of polymer/metal composite through interaction with metal particles (Sepehri et al., 2017).

In two different investigations, very good electrocatalytic activity was observed toward the oxidation of RIF (Sepehri et al., 2017) as well, INZ and EBL (Sepehri et al., 2017) by using of pre-anodized GCE coated with a nanocomposite film of poly-melamine (PMel) and AuNPs. Pre-anodized GCE which possesses many activated COOH or OH groups, was modified by melamine electropolymerization using a mix solution of HCl and melamine. PMel-modified electrode led to considerable increment in the peak currents due to more facile oxidation of RIF. More enhancement in the peak currents and nearly 100 mV negative shifts in the overpotential was also obtained from PMel/AuNPs nanocomposite owing to synergistic effects of these two materials (Sepehri et al., 2017). To prepare PMel/AuNPs layer, electrodeposition method was utilized on PMel-modified electrode immersed in a mix solution of MH_2SO_4 and $HAuCl_4$. Using PMel/AuNPs/GCE the potential shift was found to be 390 mV and 290 mV for INZ and EBL respectively (Sepehri et al., 2017).

4.2.5.5. Core-shell nanostructures. Core-shell nanostructures (CSNs) are combinatorial nanocomposites with many potential applications extending from food industry to clinic. CSNs are made up of inner (core) material(s) enclosed completely or partially (in porous CSNs) by outer layer (shell) or layers (in multi shell CSNs) of nanomaterial(s). Classifications, properties, routes of synthesis, and analytical applications of these nano structures have recently been reviewed (Kalambate et al., 2019).

Hollow CSNs, are an interesting type of CSNs in which core segment is eliminated by various tactics. In hollow mesoporous core–shell structures, mesoporous shell which provide free transmission of analytes, encapsulated the hollow core, the pooling site of the guest analytes.

Hollow core–shell nanohybrid (~58 nm diameter and 8 nm shell thickness) of manganese oxide nanoparticles and mesoporous layer of silica oxide was designed to modify home–made carbon paste microelectrode (CPME) (Gan et al., 2015). Mn_3O_4 is an inexpensive naturally abundant form of manganese oxide with substantial electrocatalytic activity but poor conductivity (Ko et al., 2014; Gan et al., 2015). The presence of Mn_3O_4 particles in this nano-composite improved the electron transfer ability and catalytic activity. This nano-modifier presented enhanced activity toward the electrocatalytic oxidation of RIF (Gan et al., 2015), relatively short accumulation time (120 s), and also proper stability (3.7% signal loss after three weeks storage). Immense experiments with hundreds-fold concentrations of 21 different potential interferents, revealed the exceptional anti interference ability of the Mn_3O_4@SiO_2/CPME nanosensor.

High level of theophylline (1,3-dimethylxanthine or TP, a drug which is frequently prescribed for patients with asthma and chronic bronchospasm (Riahi et al., 2005; Ferapontova et al., 2008)) after long treatment by INZ, can induce gastric and nervous problems (Torrent et al., 1989; Minton and Henry, 1996). Accordingly, in co-administration of these drugs, the monitoring of plasma levels by a suitable and reliable technique is of great importance in clinical chemistry. To this, researchers shaped a gold-platinum core-shell nanoparticles (Au@PtNPs)-modified GCE for simultaneous determination of INZ and TP (Gowthaman et al., 2016). Electroless deposition procedure was utilized for Au–Pt bimetallic nanoparticle fabrication. The bare electrode was first immersed in a mix solution of hydrogen tetrachloroaurate ($HAuCl_4$) and NH_2OH. Following the reduction of Au^{3+} ions by NH_2OH, AuNPs with the mean size of 43 nm and film thickness of 49 nm were formed on the surface of GCE. The deposited AuNPs, provided the nucleation center for PtNPs deposition after immersing the electrode in H_2PtCl_6/NH_2OH mix solution. The final Au@PtNPs were 80 nm spheres which formed a film with thickness of 80 nm on the surface of electrode. Au@PtNPs/GCE was able to selectively determine INZ in the presence of TP and shifted the potentials of these drugs toward less positive potentials (400 mV decrease) (Gowthaman et al., 2016).

Two significant nanomaterials are magnetic nanoparticles (MNPs) and quantum dots (QDs). A mesoporous nano-structures of polyvinylpyrrolidone (PVP), $CoFe_2O_4$MNPs (18–20 nm) and CdSeQDs was made up by Asadpour-Zeynali and his coworker for electrocatalytic

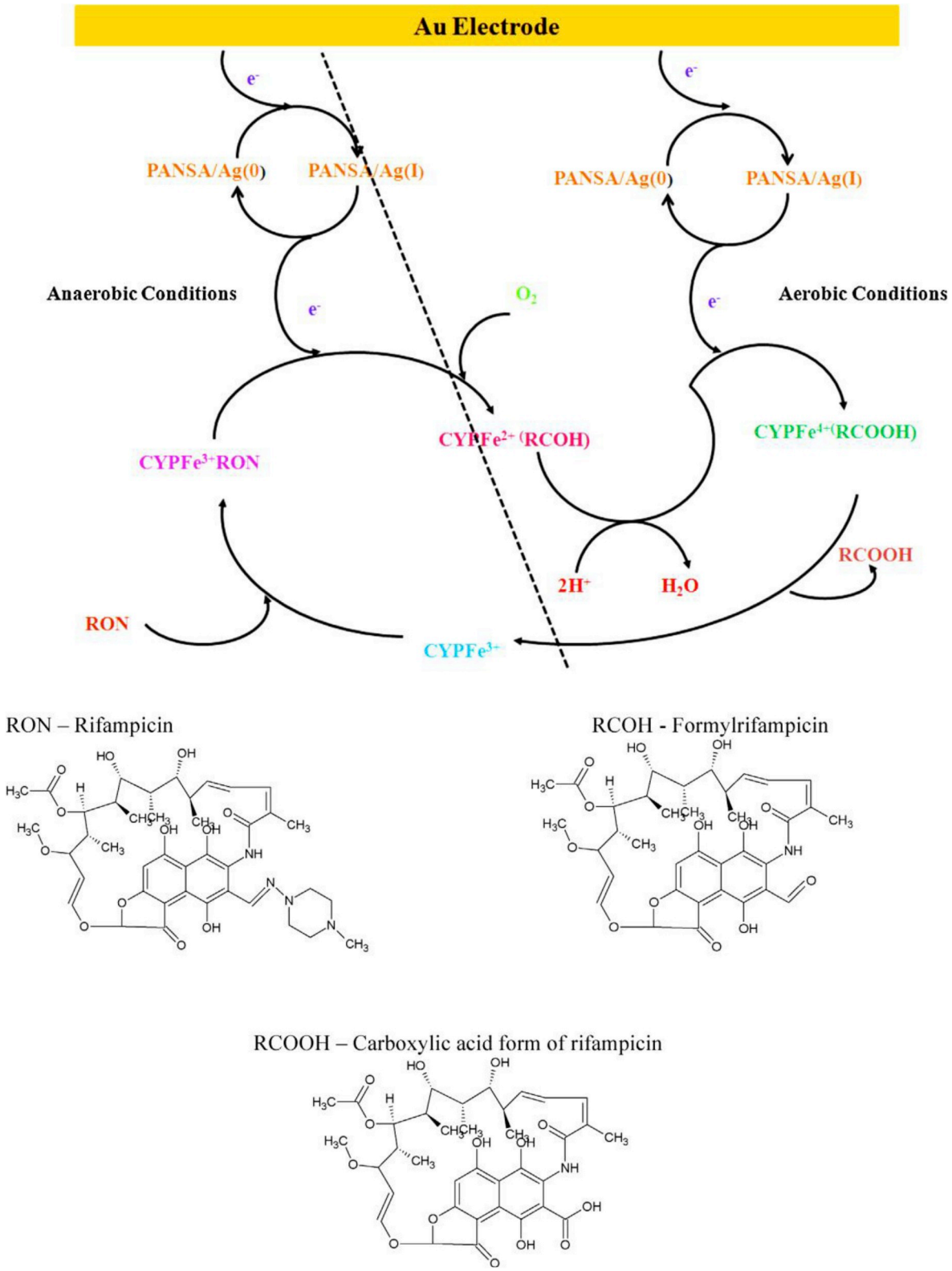

Fig. 5. Metabolism of RIF on the PVP-AgNPs/PANSA/EG-CYP2E1/AuE nanobiosensor. Reprinted with permission from Ref. (Ajayi et al., 2014).

determination of RIF using square-wave adsorptive stripping voltammetry (SWASV). PVP prevented the core segment from undesirable reactions and allowed control of the size and shape of the particles and also improved the stability with the help of an organic chelating ligand, 1, 10-phenanthroline. Higher electro-oxidation signal in comparison to the bare GCE and $CoFe_2O_4$MNPs/GCE was observed thanks to adsorptive aptitude as well as abundant active sites of the prepared nanocomposite. The sensor revealed wide LDR, good selectivity and unprecedented low LOD (4.55×10^{-17} mol^{-1}), the lowest reported value for electroanalysis of RIF up to now (Asadpour-Zeynali and Mollarasouli, 2017). In spite of the brilliant results, this device however, needs to be in excessive acidic condition (pH 2) for optimum operation.

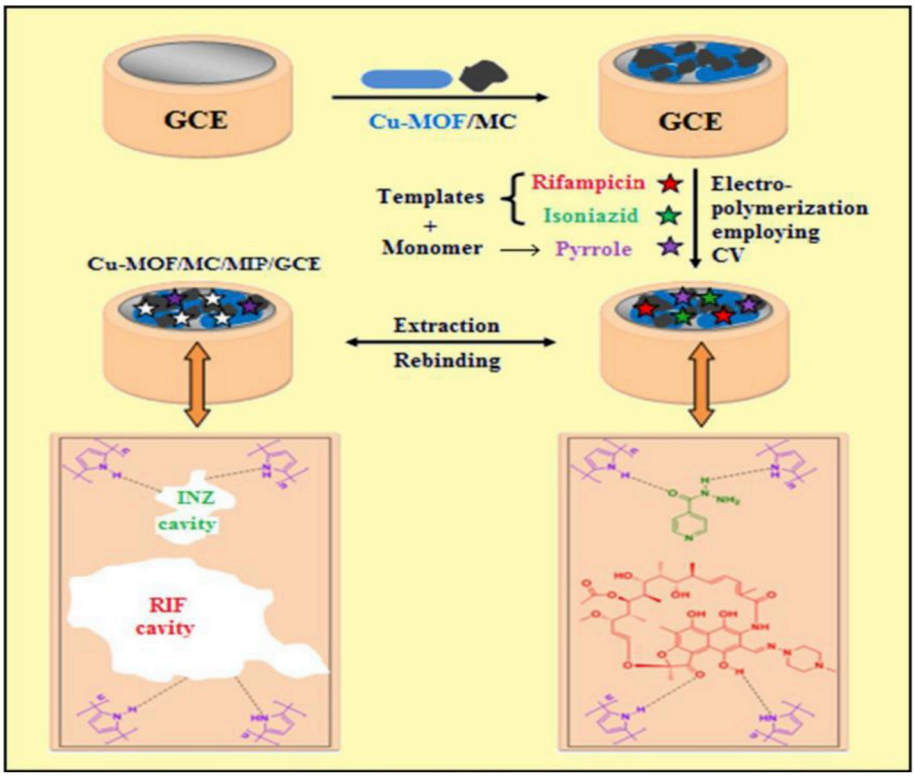

Fig. 6. Cu-MOF/MC/MIP/GCE sensor fabrication. Reprinted with permission from Ref. (Rawool and Srivastava, 2019).

Another magnetic core-shell nanostructure with related architecture was fabricated using carbon dots (C-dots) and for modification of CPE for simultaneous analysis of INZ and RIF (Shiri et al., 2017). This platform did not have the problem of acidic operational condition. Although, the LOD value obtained by this sensor was much higher in comparison to PVP capped CoFe2O4MNPs@CdSeQDs-phen/CGE device.

Another core-shell like structure was introduced for FIA based measurement of INZ in pharmaceutical formulations. Their design (Fig. 4), was comprised of SPE modified with AuNPs (10 nm)-decorated carbon nanofibers-chitosan (Nellaiappan and Kumar 2017). In comparison to (as a control), AuNPs@CNF-CHIT/SPE increased the current by 50 times and reduced the oxidation overpotential significantly (by 700 mV). Low oxidation overpotential, good reproducibility and neutral pH workability for INZ, highlight the potential applicability of the proposed technique for routine analysis of INZ in various pharmaceutical formulations. However, no biological sample was tested by the sensor and furthermore, the presence of DA and RIF showed remarkable interfering effects on INZ analysis.

4.2.6. *Multicomponent nanobio-modifiers*

In this part, we describe the recent development of the electrochemical nanobiosensors for anti-tubercular drugs quantification. The common feature of these devices is the involvement of biological (or biomimetic) recognition element (associated with nanomaterial-based matrixes) in the analysis to improve the specificity or catalytic activity.

The first RIF electrochemical biosensor, was prepared by immobilization of horseradish peroxidase (HRP) molecules on the surface of platinum electrode using PPy (Lomillo et al., 2003). Although the device was successfully applied for analysis of pharmaceutical preparations and urine samples, however, the LOD of the biosensor was in micromolar range. The biggest weakness of PPy/HRP/Pt was related to its very short lifetime which may be attributed to deleterious effect of H_2O_2 on the enzyme and PPy.

Electrodeposited nanocomposite of Poly (8-anilino-1-naphthalene sulfonic acid) (PANSA), PVP and AgNPs were used by Ajayi's group to immobilize ethylene glycol-modified cytochrome P450-2E1 (EG-CYP2E1) on the surface of gold electrode (AuE). This nanobiosensor were used for RIF determination in physiological pH, the optimum pH for CYP2E1 (Ajayi et al., 2014). The mechanism of the redox processes on this platform has been illustrated in Fig. 5. This team in their next efforts, successfully applied almost the same device with better stability for analysis of INZ (Ajayi et al., 2016).

In 2017, Chokkareddy and colleagues, developed a nanobiosensor involved HRP fixed into nanocomposite of MWCNTs and titanium oxide nanoparticles (TiO_2NPs) to enhance the analytical performance of GCE toward INZ (Chokkareddy et al., 2017a,b). After 40 and 80 days storing in 4 °C, the device lost 9% and 13% of its original electrochemical signal respectively. The sensor showed acceptable selectivity but was not subjected to analysis of any biological samples. The next nanobiosensor was fabricated by this group for measurement of RIF using Coenzyme q, a fat-soluble vitamin involved in cellular electron transport system (Ernster and Dallner, 1995). Coenzyme q was immobilized in a nanocomposite of MWCNTs and iron oxide nanoparticles (Fe3O4NPs). Voltammetric experiments with both Coenzyme q/Fe_3O_4NPs/MWCNTs- and HRP/TiO_2NPs/MWCNTs-modified GCEs showed about 8 fold increment in anodic peak currents in comparison to bare electrodes (Chokkareddy et al., 2017a,b). Despite the general weakness of biomolecules as electrode modifiers (short life time), HRP/TiO_2NPs/MWCNTs platform exhibited great stability.

Molecularly imprinted polymers (MIPs) are made by polymerization of matrix monomers in the presence of template molecule and subsequent elimination of the template. The process leads to the creation of recognition sites for specific binding of the target molecule. Thanks to biomimetic features of MIPs, they can be substitute for biological components in biosensors construction. Recently, researchers introduced a novel dual-template MIP sensor architecture which serves mesoporous carbon (MC) to improve the characteristics of copper metal organic framework (Cu-MOF) for simultaneous analysis of INZ and RIF in human urine and serum samples (Fig. 6) (Rawool and Srivastava, 2019). H and

Table 2
Electrochemical approaches for the determination of INZ and RIF.

Analyte (s)	Method (s)	Reference electrode	Working electrode	Electrode modifier (s)	LDR (M)	LOD (M)	Sensitivity (μA μM^{-1})	pH	References
INZ	SWCAdSV	SCE	HMDE	UM	0.05×10^{-8} to 0.02×10^{-4}	1.18×10^{-10}	NR	5.5	Ghoneim et al. (2003)
	DPV	SCE	AuE	UM	0.20×10^{-5} to 0.23×10^{-3}	9.69×10^{-8}	0.0019	13.68	Yun Xia and Ya Hu (2005)
	BIA-AMP	Ag/AgCl	GCE	UM	0.25×10^{-7} to 0.10×10^{-2}	0.41×10^{-8}	NR	NR[d]	Quintino and Angnes (2006)
	SWV	SCE	PtE	UM[a]	0.05×10^{-3} to 0.06×10^{-2}	NR	NR[b]	7	Gao et al. (2006)
	AMP	SCE	GCE	OPPy	3.99×10^{-6} to 12.60×10^{-2}	3.15×10^{-6}	0.084	9	Majidi et al. (2006)
	DPV	Ag/AgCl	CPE	MWCNT	0.01×10^{-4} to 0.01×10^{-1}	0.05×10^{-5}	NR	4	Shahrokhian and Amiri (2007)
	DPV	SCE	GCE	PASA	0.50×10^{-7} to 0.10×10^{-4}	0.10×10^{-7}	1.052	6.5	Yang et al. (2008)
	LSV and DPV	Ag/AgCl	GCE	UM[c]	LSV: 0.10×10^{-4} to 8.00×10^{-4} DPV: 0.05×10^{-6} to 0.85×10^{-6}	LSV: 3.94×10^{-6} DPV: 1.63×10^{-8}	NR	6	Karimi et al. (2010)
	LSV, DPV and SWV	Ag/AgCl	SPCE	PLH	LSV: 0.15×10^{-5} to 0.21×10^{-3} DPV: 0.50×10^{-6} to 0.11×10^{-3} SWV: 0.15×10^{-6} to 0.11×10^{-4}	LSV: 0.50×10^{-6} DPV: 0.17×10^{-6} SWV: 0.25×10^{-6}	LSV: 0.93 DPV: 2.99 SWV:3.71	7	Bergamini et al. (2010)
	DPV	Ag/AgCl	CPE	Surfactants: (SDS), (SDBS), (SOS), (CTAB), (TMOB), (CPB) Triton X-405 and albumin	0.94×10^{-5} to 0.99×10^{-3}	0.45×10^{-4}	NR	2	Atta et al. (2011a,b)
	LSV	Ag/AgCl	PtE	PEDOT and deferent surfactants	0.01×10^{-5} to 0.08×10^{-4} and 0.10×10^{-4} to 1.00×10^{-4}	0.32×10^{-7} and 0.45×10^{-7}	NR	7.4 and 2.3	Atta et al. (2011a,b)
	AMP	Ag/AgCl	GCE	Nf-OMC	0.10×10^{-6} to 0.37×10^{-3}	0.84×10^{-7}	0.031	7	Ratinac et al. (2011)
	CV	Ag/AgCl	GCE	Nf/Fe $(tmphen)_3^{2+}$	5.00×10^{-5} to 2.00×10^{-2}	0.13×10^{-4}	0.0025	[e]	Azad and Ganesan (2012)
	Cathodic voltammetry	Ag/AgCl	Hg(Ag)FE	UM	0.05×10^{-7} to 5.00×10^{-7}	0.41×10^{-8}	2.77 ± 0.04	3.3	Szlósarczyk et al. (2012)
	FIA-AMP	Ag/AgCl	SPE	AgNPs-HCF	0.50×10^{-5} to 0.50×10^{-3}	0.26×10^{-5}	NR	3	de Oliveira et al. (2012)
	AMP	Ag/AgCl	GCE	f-MWCNT	0.01×10^{-4} to 0.70×10^{-4}	0.27×10^{-6}	4.82	4	Chen et al. (2012)
	LSV	Ag/AgCl	GCE	ERGO	0.02×10^{-4} to 0.70×10^{-4}	0.17×10^{-6}	3.987	7	Cheemalapati et al. (2013)
	AMP	SCE	CCE	Co-FeHCFNPs/MWCNT	0.20×10^{-6} to 0.10×10^{-3}	0.80×10^{-7}	0.1149	4.5	Yu et al. (2013)
	DPV	Ag/AgCl	GCE	MWCNT/Chit	0.10×10^{-6} to 0.10×10^{-4}	0.55×10^{-7}	1.673	6.0	Satyanarayana et al. (2014)
	LSV	Ag/AgCl	GCE	RhNPs	0.70×10^{-4} to 13.00×10^{-4}	0.13×10^{-4}	0.139	7	Cheemalapati et al. (2014a, b)
	CV and BIA-AMP	Ag/AgCl	FTO	$Ni(OH)_2$), $Co(OH)_2$ and two types of NiCo $(OH)_2$	0.99×10^{-4} to 0.95×10^{-3}	Ni-100: 1.37×10^{-7} Ni-75: 5.19×10^{-8} Ni-50: 4.94×10^{-8}	By BIA-AMP: Ni-75: 0.140 Ni-100: 0.050 Co-100: 0.0894	[f]	Martins et al. (2014)
	CV	SCE	GCE	Fe $(dmbpy)_3^{2+}$/bt	1.00×10^{-5} to 1.00×10^{-2}	$0.08(\pm 0.01) \times 10^{-5}$	0.009 (±0.002)	[g]	Azad et al. (2015)
	LSV	SCE	GCE	pERGO	0.09×10^{-6} to 1.00×10^{-4}	0.15×10^{-7}	NR	7.0	Zhu et al. (2015)
	DPV	SCE	GCE	AuNPs-RGO	0.10×10^{-6} to 0.10×10^{-2}	0.10×10^{-7}	NR	7	Guo et al. (2015)
	CV	SCE	GCE	CA/GR	0.01×10^{-5} to 2.00×10^{-4}	0.03×10^{-6}	1.47488	3.5	Si et al. (2015)
	AMP	Ag/AgCl	GCE	DDQ-RGO-Nf	$0.05 \times 10^{-5}$to 3.80×10^{-4}	0.15×10^{-6}	0.420	7	Lima et al. (2016)
	SS-AMP, CV and DPV	Ag/AgCl	Au	PVP-AgNPs/PANSA/CYP2E1	0.02×10^{-4} to 0.22×10^{-4}	0.65×10^{-6}	1.25	7.4	Ajayi et al. (2016)
	CV	Ag/AgCl	CILE	PdNPs	0.50×10^{-5} to 0.10×10^{-3} and 0.15×10^{-3} to 0.26×10^{-2}	0.47×10^{-6}	NR	7	Absalan et al. (2016)
	DPV and AMP	SCE	GCE	Fe/Al-LDH	DPV: 0.49×10^{-5} to 65.00×10^{-5} AMP: 0.49×10^{-5} to 77.00×10^{-5}	DPV: 0.40×10^{-5} AMP: 0.70×10^{-5}	NR	9	Asadpour-Zeynali et al. (2016)

(*continued on next page*)

Table 2 (*continued*)

Analyte (s)	Method (s)	Reference electrode	Working electrode	Electrode modifier (s)	LDR (M)	LOD (M)	Sensitivity (μA μM^{-1})	pH	References
	CV, AMP	SCE	GCE	Ag–P(MMA-co AMPS)	AMP: 0.05×10^{-6} to 1.50×10^{-4} CV: 0.05×10^{-4} to 15.00×10^{-4}	AMP: 1.00×10^{-8} CV: 0.16×10^{-5}	AMP: 0.197 CV: 0.155	7	Rastogi et al. (2016)
	DPV	Ag/AgCl	GCE	CNT-CTAB	0.10×10^{-6} to 0.12×10^{-5}	2.14×10^{-9}	NR	4.2	Buddanavar et al. (2016)
	DPV and AMP	SCE	GCE	PEBT	DPV: 0.80×10^{-5} to 1.18×10^{-3} AMP: 2.90×10^{-5} to 1.67×10^{-3}	DPV: 0.60×10^{-5} AMP: 1.64×10^{-5}	NR	9	Asadpour-Zeynali and Arteshi (2017)
	CV and hydrodynamic AMP	SCE	PLE	PEBT	CV: 0.86×10^{-4} to 13.67×10^{-4} AMP: 0.86×10^{-4} to 6.54×10^{-4} and 8.54×10^{-4} to 22.11×10^{-4}	CV: 6.60×10^{-5} AMP: 2.04×10^{-5}	CV: 0.019568 AMP: 0.006748 and 0.003759	9	Asadpour-Zeynali and Arteshi (2017)
	FIA-AMP	Ag/AgCl	SPE	AuNPs@CNF-CHIT	0.01×10^{-4} to 0.01×10^{-1}	1.72×10^{-7}	0.0161	7	Nellaiappan and Kumar (2017)
	AMP	Ag/AgCl	GCE	GA RGO	0.05×10^{-6} to 78.31×10^{-5}	0.01×10^{-6}	2.187	7	Balasubramanian et al. (2017)
	DPV	Ag/AgCl	GCE	MWCNT-TiO_2-NPs-HRP	0.05×10^{-5} to 0.05×10^{-4}	3.35×10^{-8}	NR	7	Chokkareddy et al. (2017a, b)
	AMP	Ag/AgCl	GCE	CuMPs/GO	0.15×10^{-6} to 5.00×10^{-4}	2.34×10^{-8}	1.2394	7	Balamurugan et al. (2017)
	AMP	Ag/AgCl	GCE	FePc/f-MWCNT	0.05×10^{-4} to 4.76×10^{-4}	0.56×10^{-6}	0.023	7.4	Spindola et al. (2017)
	AMP and SWV	SCE	GCE	SnO_2NPs–RGO	AMP: 0.10×10^{-6} to 0.85×10^{-3} SWV: 0.19×10^{-7} to 0.72×10^{-5}	AMP: 0.60×10^{-7} SWV: 0.07×10^{-7}	AMP: 0.0187 SWV: 1.098	5	Santhanalkshmi and Rajesh (2018)
	AMP	Ag/AgCl	CPE	CuHCFNPs/BM	0.10×10^{-5} to 0.10×10^{-4}	0.63×10^{-7}	0.41	3.0	Oliveira et al. (2018)
	Potentiometry	Ag/AgCl	CPE	Fe_3O_4MNPs	0.10×10^{-9} to 0.10×10^{-4}	3.09×10^{-13}	NR	6.5	Shabani et al. (2018)
	FIA-AMP	Ag/AgCl	Preanodized SPCE	UM	0.10×10^{-7} to 0.10×10^{-4} 0.25×10^{-5} to 10.00×10^{-4}	0.27×10^{-8}	0.1	7.4	Gopinathan et al. (2018)
	AMP	Ag/AgCl	SPCE	B/NDMC	0.05×10^{-6} to 17.83×10^{-4}	0.15×10^{-8}	3.7058	7.0	Balasubramanian et al. (2019)
	AMP	Ag/AgCl	GCE	SnP/GRF	0.01×10^{-6} to 3.48×10^{-4}	0.10×10^{-8}	1.418	7.0	Kokulnathan et al. (2019)
INZ AA AC	DPV	Ag/AgCl	CPE	T-MWCPE	AA: 0.01×10^{-4} to 0.01×10^{-2} AC: 0.01×10^{-5} to 0.01×10^{-2} INZ: 0.01×10^{-4} to 0.01×10^{-2}	AA: 0.03×10^{-5} AC: 0.05×10^{-6} INZ: 0.05×10^{-5}	AA: 0.1584 AC: 0.3099 INZ: 0.0847	4	Shahrokhian and Asadian (2010)
INZ HDH EBH PZM	DPV	Ag/AgCl	GCE	Tyr	INZ: 0.25×10^{-4} to 12.50×10^{-4} HDH: 0.06×10^{-4} to 1.80×10^{-4} EBH: 0.20×10^{-4} to 10.00×10^{-4} PZM: 0.10×10^{-4} to 9.00×10^{-4}	INZ: 6.93×10^{-6} HDH: 5.66×10^{-6} EBH: 9.61×10^{-6} PZM: 5.13×10^{-6}	INZ:0.06 HDH: 0.228 EBH:0.09 PZM:0.165	7	Cheemalapati et al. (2014a, b)
INZ UA	DPV	SCE	GCE	PSA/ERCG	INZ: 0.05×10^{-6} to 0.15×10^{-4} UA: 0.02×10^{-6} to 0.15×10^{-4}	For both INZ and UA: 0.12×10^{-7}	0.942	9	Yan et al. (2015)
INZ BPH PZM	DPV	Ag/AgCl	GCE	PLA/GO	INZ: 0.20×10^{-4} to 14.00×10^{-4} BPH:	INZ: 2.59×10^{-6} BPH:	INZ: 0.12 BPH: 0.29 PZM: 0.43	7	Devadas et al. (2015)

(*continued on next page*)

Table 2 (*continued*)

Analyte (s)	Method (s)	Reference electrode	Working electrode	Electrode modifier (s)	LDR (M)	LOD (M)	Sensitivity (μA μM^{-1})	pH	References
					0.25×10^{-4} to 9.00×10^{-4} PZM: 0.25×10^{-4} to 16.00×10^{-4}	3.54×10^{-6} PZM: 3.28×10^{-6}			
INZ TP	DPV	Ag/AgCl	GCE	Au@PtNPs	0.50×10^{-7} to 1.00×10^{-4}	0.26×10^{-7}	NR	6	Gowthaman et al. (2016)
INZ EBH	DPV	Ag/AgCl	pre-anodized GCE	PMel-AuNPs	INZ: 0.03×10^{-5} to 17.00×10^{-5} EBH: 0.05×10^{-5} to 15.00×10^{-5}	INZ: 0.08×10^{-6} EBH: 0.21×10^{-6}	NR	7	Sepehri et al. (2017)
INZ AC	DPV	SCE	SPE	BiO Nanorods	AC: 0.05×10^{-5} to 0.97×10^{-4} 1.40×10^{-4} to 12.50×10^{-4} INZ: 0.05×10^{-4} to 1.00×10^{-4} 1.44×10^{-4} to 17.60×10^{-4}	AC: 0.30×10^{-7} INZ: 1.85×10^{-6}	AC: 0.027 and 0.0034 INZ: 0.008 and 0.0012	2	Mahmoud et al. (2017)
INZ HZN	CV	SCE	GCE	OPPy	NR	NR	NR	9	Majidi et al. (2005)
	AMP	Ag/AgCl	PCGE	AuNPs/Si Net	0.01×10^{-2} to 0.01×10^{-1}	0.01×10^{-8}	4.03 ± 0.01	9.2	Jena and Raj (2010)
	AMP	Ag/AgCl	MWCNT/GE	CoHCFNPs	INZ: 0.50×10^{-5} to 14.00×10^{-4} HZN: 0.20×10^{-5} to 12.00×10^{-4}	INZ: 0.13×10^{-5} HZN: 0.91×10^{-6}	INZ: 0.00019 HZN: 0.00034	6.5	Li et al. (2012)
INZ RIF	SWAdASV	Ag/AgCl	CPE	UM	RIF: 0.05×10^{-5} to 0.05×10^{-3} INZ: 0.05×10^{-5} to 0.04×10^{-3}	For RIF: 0.05×10^{-6} For INZ: 0.61×10^{-7}	0.211	4	Hammam et al. (2004)
	DPV	Ag/AgCl	HMDE	UM	INZ: 1.82×10^{-6} to 0.91×10^{-5} RIF: 0.48×10^{-6} to 0.24×10^{-5}	INZ: 0.36×10^{-6} RIF: 0.85×10^{-7}	NR	6.5–7	Leandro et al. (2009)
	DPP combined with SVR	Ag/AgCl	DME	UM	INZ: 0.06×10^{-6} to 0.01×10^{-2} RIF: 0.01×10^{-5} to 0.01×10^{-2}	NR	NR	7	(Asadpour-Zeynali and Soheili-Azad, 2010)
	SWV	Ag/AgCl	CPE	C-dots@$CuFe_2O_4$NPs	RIF: 0.07×10^{-6} to 0.80×10^{-5} INZ: 0.01×10^{-5} to $0.1.40 \times 10^{-5}$	RIF: 0.22×10^{-7} INZ: 0.41×10^{-7}	NR	7	Shiri et al. (2017)
	AdSDPV	Ag/AgCl	GCE	CuMOF/MC/MIP	RIF: 8.0×10^{-8} to 8.5×10^{-5} INZ: 8.0×10^{-8} to 8.5×10^{-5}	RIF: 2.8×10^{-10} INZ: 3.7×10^{-10}	RIF: 1.05 INZ:1.81	3	Rawool and Srivastava (2019)
RIF	DPP	Ag/AgCl	HMDE	UM	0.10×10^{-6} to 0.10×10^{-4}	0.10×10^{-7}	NR	4.5	Hahn and Shin (2001)
	DPAdSV and SWAdSV	Ag/AgCl	HMDE	UM	NR	DPAdSV: 61.35×10^{-10} SWAdSV: 98.28×10^{-9}	NR	3.5	Lomillo et al. (2002)
	DPAdSV	Ag/AgCl	HMDE	UM	NR	1.70×10^{-7}	NR	9.5	Alonso Lomillo et al. (2002)
	AMP	Ag/AgCl	Pt	PPy-HRP	NR	5.06×10^{-6}	NR	7	Lomillo et al. (2003)
	DPV	Ag/AgCl	CPE	DNA	At pH 5: 0 to 3.60×10^{-7} At pH 7.4: 0.20×10^{-7} to 3.00×10^{-7}	Bare CPE: 0.25×10^{-7} Modified CPE: 0.08×10^{-13}	At pH 5: 0.178 At pH 7.4: 0.5312	5 and 7.4	Girousi et al. (2004)

(*continued on next page*)

Table 2 (*continued*)

Analyte (s)	Method (s)	Reference electrode	Working electrode	Electrode modifier (s)	LDR (M)	LOD (M)	Sensitivity (μA μM^{-1})	pH	References
	AMP	Ag/AgCl	PtE	PPy/β-CD	2.61×10^{-6} to 25.23×10^{-6}	1.69×10^{-6}	NR	7.06	Lomillo et al. (2005)
	AdSV	Ag/AgCl	GCE	lead film	0.25×10^{-9} to 0.01×10^{-6}	0.09×10^{-9}	NR	5 ± 0.1	Tyszczuk and Korolczuk (2009)
	SWAdSV	Ag/AgCl	CPE	DyNW	0.10×10^{-6} to 0.10×10^{-9}	0.50×10^{-9}	NR	5	Daneshgar et al. (2009)
	LSV	Ag/AgCl	GCE	$Ni(OH)_2$NPS	peak I: 0.06×10^{-7} to 1.00×10^{-5} peak II: 0.04×10^{-6} to 0.10×10^{-4}	peak I: 4.16×10^{-9} peak II: 2.34×10^{-9}	peak I: 0.72 peak II: 1.28	7	Rastgar and Shahrokhian (2014)
	CV and DPV	Ag/AgCl	AuE[h]	PVP-AgNPs/PANSA/EG-CYP2E1	0.25×10^{-7} to 0.14×10^{-4}	0.05×10^{-6}	1.40	7.4	Ajayi et al. (2014)
	SWV	SCE	CPME	Mn_3O_4NPs@SiO_2	0.30×10^{-7} to 0.30×10^{-5}	1.08×10^{-8}	NR	6	Gan et al. (2015)
	SWASV	SCE	GCE	PVP-CoFe2O4MNPs@CdSeQDs-phen	0.10×10^{-15} to 0.10×10^{-6}	4.55×10^{-17}	NR	2.0	(Asadpour-Zeynali and Mollarasouli, 2017)
	CV and DPV	Ag/AgCl	GCE	Co en-q/Fe_3O_4NPs/MWCNTs	0.02×10^{-4} to 0.20×10^{-4}	anodic peaks I: 0.32×10^{-7} anodic peaks II: 4.13×10^{-7}	NR	7.5	Chokkareddy et al. (2017a, b)
	LSV	Ag/AgCl	GCE	PMel-AuNPs	0.08×10^{-6} to 15.00×10^{-6}	0.03×10^{-6}	NR	7	Sepehri et al. (2017)
	CV	Ag/AgCl	GCE	NiHCFNPs	0.50×10^{-5} to 0.50×10^{-3}	0.26×10^{-5}	0.12	3	de Oliveira et al. (2018)
	DPV	SCE	GCE	MWCNTs−Mo_2C	0.05×10^{-5} to 0.74×10^{-5}	0.45×10^{-7}	NR	4	Zou et al. (2018)
	LSV	SCE	GCE	MWCNTs-CoTHPP	0.01×10^{-6} to 0.50×10^{-2}	0.08×10^{-7}	0.217	4.7	Sonkar et al. (2018)
	Potentiometry	Ag/AgCl	CPE	HP-β-CD	0.32×10^{-7} to 0.22×10^{-3}	0.23×10^{-7}	NR	8.5	Dehnavi and Soleymanpour (2019)
RIF RSV	DPV-adsorptive voltammetry	Ag/AgCl	CPE	Anionic (SDS) and cationic (CTAC) surfactants	RIF: 0.35×10^{-9} to 0.54×10^{-8} RSV: 0.05×10^{-9} to 0.10×10^{-8}	In nanomolar range	NR	2/3[i]	(Gutiérrez-Fernández et al. 2004)
	(DPASV)	Ag/AgCl	PGE	UM	RIF: 1.99×10^{-8} to 11.99×10^{-7}RSV: 0.19×10^{-7} to 4.10×10^{-7}	RIF: 0.13×10^{-7}RSV: 0.60×10^{-7}	NR	2/3[j]	Kawde et al. (2014)

Abbreviations: **INZ**: isoniazid, **LDR**: linear dynamic range, **LOD**: limit of detection, **SWCAdSV:** square-wave cathodic adsorptive stripping voltammetry, **SCE**: saturated calomel electrode, **HMDE**: hanging mercury drop electrode, **UM**: un-modified, **NR**: not reported, **DPV**: differential pulse voltammetry, **AuE**: gold electrode, **BIA-AMP**: batch injection analysis with amperometry, **GCE**: glassy carbon electrode, **SWV**: square wave voltammetry, **(FcM)TMA**: (ferrocenylmethyl)trimethylammonium, **PtE**: platinum electrode, **AMP**: amperometry, **OPPy**: overoxidized polypyrrole, **CPE**: carbon paste electrode, **MWCNT**: multi-walled carbon nanotube, **PASA**: poly(amidosulfonic acid), **LSV**: linear sweep voltammetry, **SPCE**: screen printed carbon electrode, **PLH**: Poly(L-histidine), **SDS**: sodium dodecyl sulfate, **SDBS**: sodium dodecyl benzene sulfonate, **SOS**: sodium octyl sulfate, **CTAB**: cetyltrimethylammonium bromide, **TMOB**: trimethyloctylammonium bromide, **CPB**: cetylpyridinium bromide, **PEDOT**: Poly(3,4 ethylene-dioxythiophene), **Nf-OMC**: Nafion®-ordered mesoporous carbon modifier, **CV**: cyclic voltammetry, **tmphen**: 3,4,7,8-tetramethyl-1,10-phenanthroline, **Hg(Ag)FE**: cyclic renewable mercury film silver based electrode, **FIA-AMP**: flow injection analysis with amperometry, **SPE**: screen printed electrodes, **AgHCFNPs**: silver hexacyanoferrates nanoparticles, **f-MWCNT**: functionalized multi-walled carbon nanotube, **ERGO**: electrochemically reduced graphene oxide, **CCE**: composite ceramic carbon electrode, **Co-FeHCFNPs/MWCNT**: cobalt–iron hexacyanoferrate nanoparticles modified multi-walled carbon nanotubes, **Chit**: chitosan, **RhNPs**: rhodium nanoparticles, **FTO**: fluorine doped tin oxide, **Fe(dmbpy)$_3^{2+}$/bt**: $Fe(dmbpy)_3^2$ (dmbpy: 4,4′-dimethyl-2,2′-bipyridine) immobilized on bentonite clay films, **pERGO**: partially electrochemically reduced graphene oxide, **AuNPs-RGO**: gold nanoparticles/reduced graphene oxide nanocomposite, **CA/GR**: composite of cysteic acid and electrodeposited graphene, **DDQ-RGO-Nf**: 2,3-dichloro-5,6-dicyano-p-benzoquinone and reduced graphene oxide immobilized on Nafion®, **SS-AMP**: steady state amperometry, **PVP–AgNPs/PANSA/CYP2E1**: nanocomposite of polyvinylpyrrolidone, silver nanoparticles, poly (8-anilino-1-napthalene sulfonic acid) and cytochrome P450-2E1, **CILE**: carbon ionic liquid electrode, **PdNPs**: palladium nanoparticles, **LDH**: layered double hydroxides, **EIS**: electrochemical impedance spectroscopy, **Ag–P(MMA-co-AMPS)**: silver nanoparticles decorated copolymer of methyl methacrylate and 2-acrylamido-2-methylpropane sulfonic acid, **CNT-CTAB**: composite of carbon nanotubes and cetyltrimethyl ammonium bromide, **PEBT**: poly (Eriochrome black T), **PLE**: pencil lead electrode, **AuNPs@CNF-CHIT**: gold nanoparticle decorated carbon-nanofiber/chitosan hybrid, **GA RGO**: gallic acid induced reduced graphene oxide, **MWCNT-TiO_2-NPs-HRP**: nanocomposite of multi-walled carbon nanotubes, titanium oxide nanoparticles and horseradish peroxidase, **CuMPs/GO**: copper microparticles decorated graphene oxide, **FePc/f-MWCNT**: composite of graphene functionalized multi-walled carbon nanotubes and iron phthalocyanine, **SnO_2NPs–RGO**: nanocomposite of tin oxide nanoparticles and reduced graphene oxide, **CuHCFNPs/BM**: biochar-modified electrode decorated with nanostructured copper hexacyanoferrate, **Fe_3O_4MNPs**: magnetic iron oxide nanoparticles, **B/NDMC**: boron/nitrogen co-doped mesoporous carbon, **SnP/GRF**: nanocomposite **of** tin phosphate and graphene flakes, **AA**: ascorbic acid, **AC**: ascorbic acid, **T-MWCPE**: thionine immobilized multiwall carbon paste electrode, **HDH**: hydralazine hydrochloride, **EBH**: ethambutol hydrochloride, **PZM**: pyrazinamide, **Tyr**: tyrosine, **UA**: uric acid, **PSA/ERCG**: modifier layer of poly (sulfosalicylic acid) and electro-reduced carboxylated graphene, **BPH**: buspirone hydrochloride, **PLA/GO**: poly (L-arginine)/graphene oxide modifier, **TP**: theophylline, **Au@PtNPs**: gold-platinum core-shell nanoparticles, **PMel-AuNPs**: nanocomposite of poly melamine and gold nanoparticles, **HZN**: hydrazine, **PCGE**: polycrystalline gold electrode, **AuNPs/Si Net**: gold nanoparticle silicate network, **MWCNT/GE**: multi-walled carbon nanotubes/graphite composite electrode, **CoHCFNPs**: cobalt hexacyanoferrate nanoparticles, **SWAdASV**: square-wave adsorptive anodic stripping voltammetry, **RIF**: rifampicin, **DPP**: differential pulse polarography, **SVR**: support vector regression, **DME**: dropping mercury electrode, **C-dots@$CuFe_2O_4$NPs**: core-shell nanostructure of carbon dots and $CuFe_2O_4$ nanoparticles, **DPAdSV**: differential pulse adsorptive stripping voltammetry, **SWAdSV**: square-wave adsorptive stripping voltammetry, **CuMOF/MC/MIP**: molecularly imprinted polypyrrole fabricated on composite layer of copper metal organic framework and mesoporous carbon, **PPy-HRP**: horseradish peroxidase

immobilized on polypyrrole prelayer, **DNA**: deoxyribonucleic acid,**PPy/β-CD**: beta cyclodextrin immobilized into polypyrrole, **AdSV**: adsorptive stripping voltammetry, **DyNW**: dysprosium hydroxide nanowires, **RGO-Ni(OH)$_2$NPS**: nickel hydroxide nanoparticles/reduced graphene oxide nanocomposite, **PVP-AgNPs/PANSA/EG-CYP2E1**: nanocomposite of polyvinylpyrrolidone, silver nanoparticles, poly (8-anilino-1-napthalene sulfonic acid) and ethylene glycol bis (succinic acid N-hydroxysuccinimide ester)-modified cytochrome P450-2E1, **CPME**: carbon paste microelectrode, **Mn$_3$O$_4$NPs@SiO$_2$**: hollow core–shell nanohybrid of manganese oxide nanoparticles and mesoporous silica oxide, **SWASV**: square-wave adsorptive stripping voltammetry, **PVP-CoFe2O4MNPs@CdSeQDs-phen**: mesoporous core-shell nano-structures of polyvinylpyrrolidone, cobalt ferrite magnetic nanoparticles, CdSe quantum dots and 1,10-phenanthroline, **Co en-q/Fe$_3$O$_4$NPs/MWCNTs**: nanocomposite of Coenzyme q immobilized in iron oxide nanoparticles and multi-walled carbon nanotubes modifier, **NiHCFNPs**: nickel hexacyanoferrate nanoparticles, **MWCNTs—Mo$_2$C**: nanocomposite of multi-walled carbon nanotubes and molybdenum carbides, **MWCNTs-CoTHPP**: nanocomposite of multi-walled carbon nanotubes and *meso*-tetrakis(4-hydroxyphenyl)porphyrinato cobalt(II), **HP-β-CD**: 2-hydroxypropyl β-cyclodextrin, **CTAC**: cetyltrimethylammonium chloride, **RSV**: rifamycin SV, **DPASV**: differential pulse adsorptive stripping voltammetry, **PGE**: renewable pencil graphite electrode.

[a] $2.0 \times 10-4$ M (FcM) TMA as a catalyst (mediator).
[b] 0.10 M Na_2SO_4 aqueous solution as supporting electrolyte.
[c] Alizarin Red S (ARS) as a homogenous mediator.
[d] 0.1 mol L^{-1} NaOH as supporting electrolyte.
[e] In 0.1 mol L^{-1} Na_2SO_4 as supporting electrolyte.
[f] 1 mol L^{-1} KOH as supporting electrolyte.
[g] 0.1 mol L^{-1} Na_2SO_4 as supporting electrolyte.
[h] 0.0201 cm^2 gold disk electrodes.
[i] For SDS: 2 and for CTAC: 3.
[j] For RIF: 2 and for RSV: 3.

N atoms of pyrrole monomers (–NH group) they utilized, could form two hydrogen bonds with the templates (O atom of C═O group in both templates and H atom of INZ (–NH) and RIF (–OH) respectively). Their device revealed sub-nanomolar detection limit and was able to regenerate (up to 30 cycles) after each practice using template extraction procedure.

5. Conclusion

Compared with high cost sophisticated instruments, sensors are valuable detection tools in developing countries with high incidence of tuberculosis and low financial resources. In order to achieve an electrochemical sensor with maximum reusability, electrode modification should be avoided as far as possible (Karimi et al., 2010). Even though in some occasions, unmodified electrodes exhibited better performance (for example, FIA-amperometry of INZ with unmodified SPCE revealed wider LDR and much lower LOD in comparison to nanocomposite coated electrodes (Table 2)), however, high oxidation overpotential and low selectivity associated with unmodified electrodes compels the investigators to search for efficient modifiers. Many of the works reviewed here, suffered from one or more shortcomings including low stability and high detection limit and/or harsh acidic/basic condition requirement for optimum operation. INZ and RIF are usually co-administrated and in many areas, formulated in a single dosage forms. This demands the simultaneous analysis of these medicines. However, there is only a small number of reports for simultaneous determination of these agents. Up to now, there is no report of designing immunosensors (using aptamers, antibodies, etc. as biological recognition elements) and biosensing of the two drugs was limited so far to use of enzymes. Despite the encouraging results from the recent trend of combining natural biological/biomimetic elements with advanced metal- and/or carbon-based nanostructures, fabrication of such expensive complicated constructs seems to be unaffordable and unmanufacturable, particularly in many of subjected areas. Given all the above, there is still an unmet need for developing devices with inexpensive designs and better characteristics.

Declaration of competing interest

The authors declare that they have no known competing financial interests or personal relationships that could have appeared to influence the work reported in this paper.

Acknowledgement

We appreciate Dr. Javad Tashkhorian (Shiraz university) for his generous engagement in technical revision.

References

Gutiérrez-Fernández, S., Blanco-López, M., Lobo-Castañón, M.J., Miranda-Ordieres, A.J., Tuñón-Blanco, P., 2004. Adsorptive stripping voltammetry of rifamycins at unmodified and surfactant-modified carbon paste electrodes. Electroanalysis 16 (20), 1660–1666.

Absalan, G., Akhond, M., Soleimani, M., Ershadifar, H., 2016. Efficient electrocatalytic oxidation and determination of isoniazid on carbon ionic liquid electrode modified with electrodeposited palladium nanoparticles. J. Electroanal. Chem. 761, 1–7.

Agüí, L., Yáñez-Sedeño, P., Pingarrón, J.M., 2008. Role of carbon nanotubes in electroanalytical chemistry: a review. Anal. Chim. Acta 622 (1), 11–47.

Ajayan, P.M., 1993. Capillarity-induced filling of carbon nanotubes. Nature 361 (6410), 333–334.

Ajayi, R.F., Sidwaba, U., Feleni, U., Douman, S.F., Tovide, O., Botha, S., Baker, P., Fuku, X.G., Hamid, S., Waryo, T.T., 2014. Chemically amplified cytochrome P450-2E1 drug metabolism nanobiosensor for rifampicin anti-tuberculosis drug. Electrochim. Acta 128, 149–155.

Ajayi, R.F., Nxusani, E., Douman, S.F., Jonnas, A., Ntshongontshi, N., Feleni, U., Pokpas, K., Wilson, L., Iwuoha, E.I., 2016. Silver nanoparticle-doped poly (8-anilino-1-naphthalene sulphonic acid)/CYP2E1 nanobiosensor for isoniazid-A first line anti-tuberculosis drug. J. Nano Res. 44, 229–251.

Albahadily, F., Mottola, H.A., 1987. Improved response of carbon-paste electrodes for electrochemical detection in flow systems by pretreatment with surfactants. Anal. Chem. 59 (7), 958–962.

Alexa, I., Popovici, R., Ignat, M., Popovici, E., Voicu, V., 2011. Non-toxic nanocomposite containing captopril intercalated into green inorganic carrier. Digest J. Nanomater. Biostruct. 6 (3), 1091–1101.
Alonso Lomillo, M.A., Domínguez Renedo, O., Arcos Martínez, M.J., 2002. Optimization procedure, applying the experimental-design methodology, for the determination of rifampicin after metal complexation by differential pulse adsorptive stripping voltammetry. Helv. Chim. Acta 85 (8), 2430–2439.
Antiochia, R., Lavagnini, I., Magno, F., Valentini, F., Palleschi, G., 2004. Single-wall carbon nanotube paste electrodes: a comparison with carbon paste, platinum and glassy carbon electrodes via cyclic voltammetric data. Electroanalysis 16 (17), 1451–1458.
Arifa Begum, S.K., Basava Raju, D., Rama Rao, N., 2013. Simultaneous estimation of rifampicin and isoniazid in combined dosage form by a simple UV spectrophotometric method. Der Pharm. Lett. 5 (3), 419–426.
Asadpour-Zeynali, K., Arteshi, Y., 2017. Electroanalytical determination of isoniazid in pharmaceutical formulation and human plasma, using a poly (eriochrome black-T) modified pencil lead electrode. Iran. J. Anal. Chem. 4 (1), 51–58.
Asadpour-Zeynali, K., Mollarasouli, F., 2017. Novel electrochemical biosensor based on PVP capped CoFe 2 O 4@ CdSe core-shell nanoparticles modified electrode for ultra-trace level determination of rifampicin by square wave adsorptive stripping voltammetry. Biosens. Bioelectron. 92, 509–516.
Asadpour-Zeynali, K., Soheili-Azad, P., 2010. Simultaneous polarographic determination of isoniazid and rifampicin by differential pulse polarography method and support vector regression. Electrochim. Acta 55 (22), 6570–6576.
Asadpour-Zeynali, K., Shabangoli, Y., Nejati, K., 2016. Electrochemical synthesis of Fe/Al-layered double hydroxide on a glassy carbon electrode: application for electrocatalytic reduction of isoniazid. J. Iran. Chem. Soc. 13 (1), 29–36.
Atta, N.F., Galal, A., Abu-Attia, F.M., Azab, S.M., 2011. Characterization and electrochemical investigations of micellar/drug interactions. Electrochim. Acta 56 (5), 2510–2517.
Atta, N.F., Galal, A., Ahmed, R.A., 2011. Voltammetric behavior and determination of isoniazid using PEDOT electrode in presence of surface active agents. Int. J. Electrochem. Sci. 6 (10), 5097–5113.
Azad, U.P., Ganesan, V., 2012. Efficient electrocatalytic oxidation and selective determination of isoniazid by Fe (tmphen) 32+-exchanged Nafion®-modified electrode. J. Solid State Electrochem. 16 (9), 2907–2911.
Azad, U.P., Prajapati, N., Ganesan, V., 2015. Selective determination of isoniazid using bentonite clay modified electrodes. Bioelectrochemistry 101, 120–125.
Balamurugan, T., Manibalan, K., Chen, S.M., Balasubramnian, P., Huang, S.-T., 2017. High sensitive electrochemical quantification of isoniazid in biofluids using copper particles decorated graphene oxide nano composite. Int. J. Electrochem. Sci. 12 (10), 9150–9160.
Balasubramanian, P., Thirumalraj, B., Chen, S.-M., Barathi, P., 2017. Electrochemical determination of isoniazid using gallic acid supported reduced graphene oxide. J. Electrochem. Soc. 164 (7), H503–H508.
Balasubramanian, P., Balamurugan, T., Chen, S.-M., Chen, T.-W., Lin, P.-H.J.S., Chemical, A.B., 2019. A novel, efficient electrochemical sensor for the detection of isoniazid based on the B/N doped mesoporous carbon modified electrode. Sens. Actuators B Chem. 283, 613–620.
Bano, K., Bajwa, S.Z., Bassous, N.J., Webster, T.J., Shaheen, A., Taj, A., Hameed, S., Tehseen, B., Dai, Z., Iqbal, M.Z., 2019. Development of biocompatible 1D CuO nanoneedles and their potential for sensitive, mass-based detection of anti-tuberculosis drugs. Appl. Nanosci. 1–11.
Baś, B., 2006. Refreshable mercury film silver based electrode for determination of chromium (VI) using catalytic adsorptive stripping voltammetry. Anal. Chim. Acta 570 (2), 195–201.
Baś, B., Kowalski, Z., 2002. Preparation of silver surface for mercury film electrode of prolonged analytical application. Electroanalysis 14 (15-16), 1067–1071.
Bergamini, M.F., dos Santos, D.P., Zanoni, M.V.B., 2007. Development of a voltammetric sensor for chromium (VI) determination in wastewater sample. Sens. Actuators B Chem. 123 (2), 902–908.
Bergamini, M.F., Santos, D.P., Zanoni, M.V.B., 2010. Determination of isoniazid in human urine using screen-printed carbon electrode modified with poly-L-histidine. Bioelectrochemistry 77 (2), 133–138.
Brown, K.R., Natan, M.J., 1998. Hydroxylamine seeding of colloidal Au nanoparticles in solution and on surfaces. Langmuir 14 (4), 726–728.
Brunetti, B., Desimoni, E., 2009. Determination of theophylline at a cysteic acid modified glassy carbon electrode. Electroanalysis 21 (6), 772–778.
Buddanavar, A.T., Gowda, J.I., Nandibewoor, S.T., 2016. Voltammetric behavior of isoniazid and its electroanalytical determination at carbon nanotubes-CTAB modified glassy carbon electrode. Anal. Bioanal. Electrochem. 8 (3), 329–344.
Calvori, C., Frontali, L., Leoni, L., Tecce, G., 1965. Effect of rifamycin on protein synthesis. Nature 207 (4995), 417–418.
Campbell, E.A., Korzheva, N., Mustaev, A., Murakami, K., Nair, S., Goldfarb, A., Darst, S. A., 2001. Structural mechanism for rifampicin inhibition of bacterial RNA polymerase. Cell 104 (6), 901–912.
Cao, L., Li, Z., Su, K., Cheng, B., 2016. Hydrophilic Graphene Preparation from Gallic Acid Modified Graphene Oxide in Magnesium Self-Propagating High Temperature Synthesis Process, vol. 6. Scientific reports.
Chandra, U., Swamy, B.K., Gilbert, O., Sherigara, B., 2010. Determination of dopamine in presence of ascorbic acid at eriochrome black t modified carbon paste electrode: a voltammetric study. Int. J. Electrochem. Sci. 5 (10), 1475–1483.
Chang, T.K., Yu, L., Maurel, P., Waxman, D.J., 1997. Enhanced cyclophosphamide and ifosfamide activation in primary human hepatocyte cultures: response to cytochrome P-450 inducers and autoinduction by oxazaphosphorines. Cancer Res. 57 (10), 1946–1954.
Chang, K.C., Leung, C.C., Yew, W.W., Tam, C.M., 2007. Standard anti-tuberculosis treatment and hepatotoxicity: do dosing schedules matter? Eur. Respir. J. 29 (2), 347–351.
Chawla, P.K., Udwadia, Z.F., Soman, R., Mahashur, A.A., Amale, R.A., Dherai, A.J., Lokhande, R.V., Naik, P.R., Ashavaid, T.F., 2016. Importance of therapeutic drug monitoring of rifampicin. J. Assoc. Phys. India 64, 68–72.
Cheemalapati, S., Palanisamy, S., Chen, S.-M., 2013. Electrochemical determination of isoniazid at electrochemically reduced graphene oxide modified electrode. Int. J. Electrochem. Sci. 8 (3), 3.
Cheemalapati, S., Chen, S.-M., Ali, M.A., Al-Hemaid, F.M., 2014. Enhanced electrocatalytic oxidation of isoniazid at electrochemically modified rhodium electrode for biological and pharmaceutical analysis. Colloids Surfaces B Biointerfaces 121, 444–450.
Cheemalapati, S., Devadas, B., Chen, S.-M., Ali, M.A., Al-Hemaid, F.M., 2014. Electrochemical determination of selected antihypertensive and antituberculosis drugs at a tyrosine-modified electrode. Anal. Methods 6 (17), 6774–6782.
Chen, W.-C., Unnikrishnan, B., Chen, S.-M., 2012. Electrochemical oxidation and amperometric determination of isoniazid at functionalized multiwalled carbon nanotube modified electrode. Int. J. Electrochem. Sci. 7, 9138–9149.
Chokkareddy, R., Bhajanthri, N.K., Redhi, G.G., 2017. An enzyme-induced novel biosensor for the sensitive electrochemical determination of isoniazid. Biosensors 7 (2), 21.
Chokkareddy, R., Bhajanthri, N.K., Redhi, G.G., 2017. A novel electrode architecture for monitoring rifampicin in various pharmaceuticals. Int. J. Electrochem. Sci. 12, 9190–9203.
Chouchane, S., Lippai, I., Magliozzo, R.S., 2000. Catalase-peroxidase (Mycobacterium tuberculosis KatG) catalysis and isoniazid activation. Biochemistry 39 (32), 9975–9983.
Collins, R.D., 1985. Atlas of Drug Reactions. Churchill Livingstone.
Control, C.f.D., Prevention, 2000. Updated guidelines for the use of rifabutin or rifampin for the treatment and prevention of tuberculosis among HIV-infected patients taking protease inhibitors or nonnucleoside reverse transcriptase inhibitors. MMWR. Morb. Mortal. Wkly. Rep. 49 (9), 185.
Daneshgar, P., Norouzi, P., Dousty, F., Ganjali, M.R., Moosavi-Movahedi, A.A., 2009. Dysprosium hydroxide nanowires modified electrode for determination of rifampicin drug in human urine and capsules by adsorptive square wave voltammetry. Curr. Pharmaceut. Anal. 5 (3), 246–255.
de Oliveira, P.R., Oliveira, M.M., Zarbin, A.J., Marcolino-Junior, L.H., Bergamini, M.F., 2012. Flow injection amperometric determination of isoniazid using a screen-printed carbon electrode modified with silver hexacyanoferrates nanoparticles. Sens. Actuators B Chem. 171, 795–802.
de Oliveira, P.R., Schibelbain, A.F., Neiva, E.G., Zarbin, A.J., Bergamini, M.F., 2018. Nickel Hexacyanoferrate Supported at Nickel Nanoparticles for Voltammetric Determination of Rifampicin. Sensors and Actuators B: Chemical.
Dehnavi, A., Soleymanpour, A., 2019. New chemically modified carbon paste sensor for nanomolar concentration measurement of rifampicin in biological and pharmaceutical media. Mater. Sci. Eng. C 94, 403–409.
Devadas, B., Cheemalapati, S., Chen, S.-M., Ali, M.A., Al-Hemaid, F.M., 2015. Highly sensing graphene oxide/poly-arginine-modified electrode for the simultaneous electrochemical determination of buspirone, isoniazid and pyrazinamide drugs. Ionics 21 (2), 547–555.
Du, J., Yue, R., Ren, F., Yao, Z., Jiang, F., Yang, P., Du, Y., 2014. Novel graphene flowers modified carbon fibers for simultaneous determination of ascorbic acid, dopamine and uric acid. Biosens. Bioelectron. 53, 220–224.
El-Yazigi, A., Raines, D.A., 1992. Simultaneous microdetermination of rifampin, deacetylrifampin, isoniazid, and acetylisoniazid in plasma by liquid chromatography with dual electrochemical and spectrophotometric detection. Pharm. Res. 9 (6), 812–816.
Ernster, L., Dallner, G., 1995. Biochemical, physiological and medical aspects of ubiquinone function. Biochim. Biophys. Acta (BBA) - Mol. Basis Dis. 1271 (1), 195–204.
Faria, A.F., De Souza, M.V., Bruns, R.E., De Oliveira, M.A., 2010. Simultaneous determination of first-line anti-tuberculosis drugs by capillary zone electrophoresis using direct UV detection. Talanta 82 (1), 333–339.
Ferapontova, E.E., Olsen, E.M., Gothelf, K.V., 2008. An RNA aptamer-based electrochemical biosensor for detection of theophylline in serum. J. Am. Chem. Soc. 130 (13), 4256–4258.
Ferreira, L., Felix, F.S., Angnes, L., 2012. Fast determination of ciclopirox in pharmaceutical products by amperometry in flow and batch injection systems. Electroanalysis 24 (4), 961–966.
Forrest, G.N., Tamura, K., 2010. Rifampin combination therapy for nonmycobacterial infections. Clin. Microbiol. Rev. 23 (1), 14–34.
Gan, T., Shi, Z., Wang, K., Sun, J., Lv, Z., Liu, Y., 2015. Rifampicin determination in human serum and urine based on a disposable carbon paste microelectrode modified with a hollow manganese oxide@ mesoporous silica oxide core-shell nanohybrid. Can. J. Chem. 93 (10), 1061–1068.
Gangadharam, P., Mitchison, D., Subbaiah, T., Short, E.I., 1958. The detection of isoniazid in urine. Tubercle 39 (4), 191–200.
Gao, Z.-N., Han, X.-X., Yao, H.-Q., Liang, B., Liu, W.-Y., 2006. Electrochemical oxidation of isoniazid catalyzed by (FcM) TMA at the platinum electrode and its practical analytical application. Anal. Bioanal. Chem. 385 (7), 1324–1329.
Ghica, M.E., Pauliukaite, R., Fatibello-Filho, O., Brett, C.M., 2009. Application of functionalised carbon nanotubes immobilised into chitosan films in amperometric enzyme biosensors. Sens. Actuators B Chem. 142 (1), 308–315.
Ghoneim, M., El-Baradie, K., Tawfik, A., 2003. Electrochemical behavior of the antituberculosis drug isoniazid and its square-wave adsorptive stripping

voltammetric estimation in bulk form, tablets and biological fluids at a mercury electrode. J. Pharm. Biomed. Anal. 33 (4), 673–685.
Gilbert, D.N., 2011. The Sanford guide to antimicrobial therapy 2011. Antimicrob. Ther. 4–62.
Girousi, S.T., Gherghi, I.C., Karava, M., 2004. DNA-modified carbon paste electrode applied to the study of interaction between Rifampicin (RIF) and DNA in solution and at the electrode surface. J. Pharm. Biomed. Anal. 36 (4), 851–858.
Glass, B., Agatonovic-Kustrin, S., Chen, Y.-J., Wisch, M., 2007. Optimization of a stability-indicating HPLC method for the simultaneous determination of rifampicin, isoniazid, and pyrazinamide in a fixed-dose combination using artificial neural networks. J. Chromatogr. Sci. 45 (1), 38–44.
Gopinathan, M., Thiyagarajan, N., Thiruppathi, M., Zen, J.M.J.E., 2018. Electrocatalytic oxidation and flow injection analysis of isoniazid drug using an unmodified screen printed carbon electrode in neutral pH. Electroanalysis 30 (7), 1400–1406.
Gowthaman, N., Kesavan, S., John, S.A., 2016. Monitoring isoniazid level in human fluids in the presence of theophylline using gold@ platinum core@ shell nanoparticles modified glassy carbon electrode. Sens. Actuators B Chem. 230, 157–166.
Güell, A.G., Meadows, K.E., Unwin, P.R., Macpherson, J.V., 2010. Trace voltammetric detection of serotonin at carbon electrodes: comparison of glassy carbon, boron doped diamond and carbon nanotube network electrodes. Phys. Chem. Chem. Phys. 12 (34), 10108–10114.
Guo, H.-L., Wang, X.-F., Qian, Q.-Y., Wang, F.-B., Xia, X.-H., 2009. A green approach to the synthesis of graphene nanosheets. ACS Nano 3 (9), 2653–2659.
Guo, Z., Wang, Z.-y., Wang, H.-h., Huang, G.-q., Li, M.-m., 2015. Electrochemical sensor for Isoniazid based on the glassy carbon electrode modified with reduced graphene oxide–Au nanomaterials. Mater. Sci. Eng. C 57, 197–204.
Hahn, Y., Shin, S., 2001. Electrochemical behavior and differential pulse polarographic determination of rifampicin in the pharmaceutical preparations. Arch Pharm. Res. (Seoul) 24 (2), 100.
Hammam, E., Beltagi, A., Ghoneim, M., 2004. Voltammetric assay of rifampicin and isoniazid drugs, separately and combined in bulk, pharmaceutical formulations and human serum at a carbon paste electrode. Microchem. J. 77 (1), 53–62.
Hasebe, Y., Akiyama, T., Yagisawa, T., Uchiyama, S., 1998. Enzyme-less amperometric biosensor for l-ascorbate using poly-l-histidine-copper complex as an alternative biocatalyst. Talanta 47 (5), 1139–1147.
Heitner-Wirguin, C., 1996. Recent advances in perfluorinated ionomer membranes: structure, properties and applications. J. Membr. Sci. 120 (1), 1–33.
Hernandez, Y., Nicolosi, V., Lotya, M., Blighe, F.M., Sun, Z., De, S., McGovern, I., Holland, B., Byrne, M., Gun'Ko, Y.K., 2008. High-yield production of graphene by liquid-phase exfoliation of graphite. Nat. Nanotechnol. 3 (9), 563–568.
Ho, K.-C., Yeh, W.-M., Tung, T.-S., Liao, J.-Y., 2005. Amperometric detection of morphine based on poly (3, 4-ethylenedioxythiophene) immobilized molecularly imprinted polymer particles prepared by precipitation polymerization. Anal. Chim. Acta 542 (1), 90–96.
Hu, G., Guo, Y., Shao, S., 2009. Ultrasensitive electrochemical sensing of the anticancer drug tirapazamine using an ordered mesoporous carbon modified pyrolytic graphite electrode. Biosens. Bioelectron. 24 (11), 3391–3394.
Hüger, E., Osuch, K., 2004. Ferromagnetism in body centred cubic Rh. Solid State Commun. 131 (3), 175–179.
Jena, B.K., Raj, C.R., 2010. Au nanoparticle decorated silicate network for the amperometric sensing of isoniazid. Talanta 80 (5), 1653–1656.
Kalambate, P.K., Huang, Z., Li, Y., Shen, Y., Xie, M., Huang, Y., Srivastava, A.K., 2019. Core@ shell nanomaterials based sensing devices: a review. Trac. Trends Anal. Chem. 115, 147–161.
Karimi, M.A., Hatefi-Mehrjardi, A., Mazloum-Ardakani, M., Behjatmanesh-Ardakani, R., Mashhadizadeh, M.H., Sargazi, S., 2010. Study of electrocatalytic oxidation of isoniazid drug using Alizarin Red S as a mediator on the glassy carbon electrode. Int. J. Electrochem. Sci. 5 (11), 1634–1648.
Kawde, A.-N., Temerk, Y., Farhan, N., 2014. Adsorptive stripping voltammetry of antibiotics rifamycin SV and rifampicin at renewable pencil electrodes. Acta Chim. Slov. 61 (2).
Khuhawar, M., Zardari, L., 2006. Capillary gas chromatographic determination of isoniazid in pharmaceutical preparations and blood by precolumn derivatization with trifluoroacetylacetone. J. Food Drug Anal. 14 (4).
Kim, S.W., Kim, T., Kim, Y.S., Choi, H.S., Lim, H.J., Yang, S.J., Park, C.R., 2012. Surface modifications for the effective dispersion of carbon nanotubes in solvents and polymers. Carbon 50 (1), 3–33.
Ko, Y.N., Park, S.B., Choi, S.H., Kang, Y.C., 2014. One-pot synthesis of manganese oxide-carbon composite microspheres with three dimensional channels for Li-ion batteries. Sci. Rep. 4, 5751.
Kokulnathan, T., Suvina, V., Wang, T.-J., Balakrishna, G.R., 2019. Synergistic design of tin phosphate entrapped graphene flakes nanocomposite as an efficient catalyst for the electrochemical determination of antituberculosis drug isoniazid in biological samples. Inorg. Chem. Front. 6, 1831–1841.
Korolczuk, M., Tyszczuk, K., 2006. Application of lead film electrode for simultaneous adsorptive stripping voltammetric determination of Ni (II) and Co (II) as their nioxime complexes. Anal. Chim. Acta 580 (2), 231–235.
Korolczuk, M., Tyszczuk, K., 2007. Determination of folic acid by adsorptive stripping voltammetry at a lead film electrode. Electroanalysis 19 (18), 1959–1962.
Korolczuk, M., Tyszczuk, K., Grabarczyk, M., 2005. Adsorptive stripping voltammetry of nickel and cobalt at in situ plated lead film electrode. Electrochem. Commun. 7 (12), 1185–1189.
Korrapati, S., Muneppa, C., Pullela, P.K., Shivashankar, G.K., Vijayalakshmi, U., 2017. Objective measurement of isoniazid levels: practical approach for monitoring tuberculosis drug treatment adherence. IET Nanobiotechnol. 11 (7), 821–826.
Kumar, S.S., Mathiyarasu, J., Phani, K.L., 2005. Exploration of synergism between a polymer matrix and gold nanoparticles for selective determination of dopamine. J. Electroanal. Chem. 578 (1), 95–103.
Lapa, R.A., Lima, J.L., Santos, J.L., 2000. Fluorimetric determination of isoniazid by oxidation with cerium (IV) in a multicommutated flow system. Anal. Chim. Acta 419 (1), 17–23.
Leandro, K.C., Carvalho, J.M.d., Giovanelli, L.F., Moreira, J.C., 2009. Development and validation of an electroanalytical methodology for determination of isoniazid and rifampicin content in pharmaceutical formulations. Braz. J. Pharmaceut. Sci. 45 (2), 331–337.
Li, B., He, Y., Lv, J., Zhang, Z., 2005. Simultaneous determination of rifampicin and isoniazid by continuous-flow chemiluminescence with artificial neural network calibration. Anal. Bioanal. Chem. 383 (5), 817–824.
Li, Y., Shi, X., Hao, J., 2006. Electrochemical behavior of glassy carbon electrodes modified by multi-walled carbon nanotube/surfactant films in a buffer solution and an ionic liquid. Carbon 44 (13), 2664–2670.
Li, X., Chen, Z., Zhong, Y., Yang, F., Pan, J., Liang, Y., 2012. Cobalt hexacyanoferrate modified multi-walled carbon nanotubes/graphite composite electrode as electrochemical sensor on microfluidic chip. Anal. Chim. Acta 710, 118–124.
Lim, C.X., Hoh, H.Y., Ang, P.K., Loh, K.P., 2010. Direct voltammetric detection of DNA and pH sensing on epitaxial graphene: an insight into the role of oxygenated defects. Anal. Chem. 82 (17), 7387–7393.
Lima, K.C.M.S., Santos, A.C.F., Fernandes, R.N., Damos, F.S., Luz, R.d.C.S., 2016. Development of a novel sensor for isoniazid based on 2, 3-dichloro-5, 6-dicyano-p-benzoquinone and graphene: application in drug samples utilized in the treatment of tuberculosis. Microchem. J. 128, 226–234.
Lin, X.-Q., Jin, G.-P., 2005. Monolayer modification of glassy carbon electrode by using propionylcholine for selective detection of uric acid. Electrochim. Acta 50 (16), 3210–3216.
Liu, J., Sun, J., Zhang, W., Gao, K., He, Z., 2008. HPLC determination of rifampicin and related compounds in pharmaceuticals using monolithic column. J. Pharm. Biomed. Anal. 46 (2), 405–409.
Lokesh, K., Shivaraj, Y., Dayananda, B., Chandra, S., 2009. Synthesis of phthalocyanine stabilized rhodium nanoparticles and their application in biosensing of cytochrome c. Bioelectrochemistry 75 (2), 104–109.
Lomillo, A., Domínguez Renedo, O., Arcos Martínez, M., 2002. Optimization of the experimental parameters in the determination of rifampicin by adsorptive stripping voltammetry. Electroanalysis 14 (9), 634–637.
Lomillo, M.A., Kauffmann, J., Martinez, M.A., 2003. HRP-based biosensor for monitoring rifampicin. Biosens. Bioelectron. 18 (9), 1165–1171.
Lomillo, M.A.A., Renedo, O.D., Martínez, M.J.A., 2005. Optimization of a cyclodextrin-based sensor for rifampicin monitoring. Electrochim. Acta 50 (9), 1807–1811.
Lu, Q., Dong, X., Li, L.-J., Hu, X., 2010. Direct electrochemistry-based hydrogen peroxide biosensor formed from single-layer graphene nanoplatelet–enzyme composite film. Talanta 82 (4), 1344–1348.
Lund, W., 1994. The Pharmaceutical Codex, Principle and Practice of Pharmaceutics.
Madan, J., Dwivedi, A., Singh, S., 2005. Estimation of antitubercular drugs combination in pharmaceutical formulations using multivariate calibration. Anal. Chim. Acta 538 (1), 345–353.
Mahmoud, B.G., Khairy, M., Rashwan, F.A., Banks, C.E., 2017. Simultaneous voltammetric determination of acetaminophen and isoniazid (Hepatotoxicity-Related drugs) utilizing bismuth oxide nanorod modified screen-printed electrochemical sensing platforms. Anal. Chem. 89 (3), 2170–2178.
Majidi, M.R., Jouyban, A., Asadpour-Zeynali, K., 2005. Genetic algorithm based potential selection in simultaneous voltammetric determination of isoniazid and hydrazine by using partial least squares (PLS) and artificial neural networks (ANNs). Electroanalysis 17 (10), 915–918.
Majidi, M.R., Jouyban, A., Asadpour-Zeynali, K., 2006. Voltammetric behavior and determination of isoniazid in pharmaceuticals by using overoxidized polypyrrole glassy carbon modified electrode. J. Electroanal. Chem. 589 (1), 32–37.
Martins, P.R., Ferreira, L.M.C., Araki, K., Angnes, L., 2014. Influence of cobalt content on nanostructured alpha-phase-nickel hydroxide modified electrodes for electrocatalytic oxidation of isoniazid. Sens. Actuators B Chem. 192, 601–606.
Maru, G.B., Bhide, S.V., 1982. Effect of antioxidants and antitoxicants of isoniazid on the formation of lung tumours in mice by isoniazid and hydrazine sulphate. Cancer Lett. 17 (1), 75–80.
Mauritz, K.A., Moore, R.B., 2004. State of understanding of nafion. Chem. Rev. 104 (10), 4535–4586.
Merkoçi, A., 2006. Carbon nanotubes in analytical sciences. Microchim. Acta 152 (3), 157–174.
Minton, N.A., Henry, J.A., 1996. Treatment of theophylline overdose. Am. J. Emerg. Med. 14 (6), 606–612.
Mishra, P., Albiol-Chiva, J., Bose, D., Durgbanshi, A., Peris-Vicente, J., Carda-Broch, S., Esteve-Romero, J., 2018. Optimization and validation of a chromatographic method for the quantification of isoniazid in urine of tuberculosis patients according to the european medicines agency guideline. Antibiotics 7 (4), 107.
Mola, S.J., Nield, L.S., Weisse, M.E., 2008. Treatment and prevention of N meningitidis infection. Infect. Med. 25 (3).
Mousty, C., 2004. Sensors and biosensors based on clay-modified electrodes—new trends. Appl. Clay Sci. 27 (3), 159–177.
Muchindu, M., Waryo, T., Arotiba, O., Kazimierska, E., Morrin, A., Killard, A.J., Smyth, M.R., Jahed, N., Kgarebe, B., Baker, P.G., 2010. Electrochemical nitrite nanosensor developed with amine-and sulphate-functionalised polystyrene latex beads self-assembled on polyaniline. Electrochim. Acta 55 (14), 4274–4280.
Munawar, A., Schirhagl, R., Rehman, A., Shaheen, A., Taj, A., Bano, K., Bassous, N.J., Webster, T.J., Khan, W.S., Bajwa, S.Z., 2019. Facile in situ generation of bismuth

tungstate nanosheet-multiwalled carbon nanotube composite as unconventional affinity material for quartz crystal microbalance detection of antibiotics. J. Hazard Mater. 373, 50–59.
Murugesan, S., Myers, K., Subramanian, V.R., 2011. Amino-functionalized and acid treated multi-walled carbon nanotubes as supports for electrochemical oxidation of formic acid. Appl. Catal. B Environ. 103 (3), 266–274.
Nagaraja, P., Murthy, K.S., Yathirajan, H., 1996. Spectrophotometric determination of isoniazid with sodium 1, 2-naphthoquinone-4-sulphonate and cetyltrimethyl ammonium bromide. Talanta 43 (7), 1075–1080.
Neiva, E.G., Bergamini, M.F., Oliveira, M.M., Marcolino Jr., L.H., Zarbin, A.J., 2014. PVP-capped nickel nanoparticles: synthesis, characterization and utilization as a glycerol electrosensor. Sens. Actuators B Chem. 196, 574–581.
Neiva, E.G., Oliveira, M.M., Bergamini, M.F., Marcolino Jr., L.H., Zarbin, A.J., 2016. One material, multiple functions: graphene/Ni (OH) 2 thin films applied in batteries, electrochromism and sensors. Sci. Rep. 6, 33806.
Nellaiappan, S., Kumar, A.S., 2017. Electrocatalytic oxidation and flow injection analysis of isoniazid drug using a gold nanoparticles decorated carbon nanofibers-chitosan modified carbon screen printed electrode in neutral pH. J. Electroanal. Chem. 801, 171–178.
Notterman, D.A., Nardi, M., Saslow, J.G., 1986. Effect of dose formulation on isoniazid absorption in two young children. Pediatrics 77 (6), 850–852.
Oliveira, P.R., Kalinke, C., Mangrich, A.S., Marcolino-Junior, L.H., Bergamini, M.F., 2018. Copper hexacyanoferrate nanoparticles supported on biochar for amperometric determination of isoniazid. Electrochim. Acta 285, 373–380.
Palanisamy, S., Unnikrishnan, B., Chen, S.-M., 2012. An amperometric biosensor based on direct immobilization of horseradish peroxidase on electrochemically reduced graphene oxide modified screen printed carbon electrode. Int. J. Electrochem. Sci. 7, 7935–7947.
Palmisano, F., Malitesta, C., Centonze, D., Zambonin, P., 1995. Correlation between permselectivity and chemical structure of overoxidized polypyrrole membranes used in electroproduced enzyme biosensors. Anal. Chem. 67 (13), 2207–2211.
Phillips, G.O., Williams, P.A., 2009. Handbook of Hydrocolloids. Elsevier.
Piech, R., 2008. Determination of selenium traces on cyclic renewable mercury film silver electrode in presence of copper ions using cathodic stripping voltammetry. Electroanalysis 20 (22), 2475–2481.
Piech, R., 2011. Study on simultaneous measurements of trace gallium (III) and germanium (IV) by adsorptive stripping voltammetry using mercury film electrode. J. Appl. Electrochem. 41 (2), 207–214.
Piech, R., Baś, B., Kubiak, W.W., 2007. The cyclic renewable mercury film silver based electrode for determination of uranium (VI) traces using adsorptive stripping voltammetry. Electroanalysis 19 (22), 2342–2350.
Piech, R., Baś, B., Kubiak, W.W., 2008. The cyclic renewable mercury film silver based electrode for determination of molybdenum (VI) traces using adsorptive stripping voltammetry. Talanta 76 (2), 295–300.
Prasanthi, B., Ratna, J.V., Phani, R.C., 2015. Development and validation of RP-HPLC method for simultaneous estimation of rifampicin, isoniazid and pyrazinamide in human plasma. J. Anal. Chem. 70 (8), 1015–1022.
Quintino, M.S., Angnes, L., 2004. Batch injection analysis: an almost unexplored powerful tool. Electroanalysis 16 (7), 513–523.
Quintino, M.S., Angnes, L., 2004. Bia-amperometric quantification of salbutamol in pharmaceutical products. Talanta 62 (2), 231–236.
Quintino, M.S., Angnes, L., 2006. Fast BIA-amperometric determination of isoniazid in tablets. J. Pharm. Biomed. Anal. 42 (3), 400–404.
Quintino, M.S., Araki, K., Toma, H.E., Angnes, L., 2002. Batch injection analysis utilizing modified electrodes with tetraruthenated porphyrin films for acetaminophen quantification. Electroanalysis 14 (23), 1629–1634.
Ramappa, V., Aithal, G.P., 2013. Hepatotoxicity related to anti-tuberculosis drugs: mechanisms and management. J. Clin. Exp. Hepatol. 3 (1), 37–49.
Rana, F., 2013. Rifampicin—an overview. IJRPC 3 (1), 83–87.
Rastgar, S., Shahrokhian, S., 2014. Nickel hydroxide nanoparticles-reduced graphene oxide nanosheets film: layer-by-layer electrochemical preparation, characterization and rifampicin sensory application. Talanta 119, 156–163.
Rastogi, P.K., Ganesan, V., Azad, U.P., 2016. Electrochemical determination of nanomolar levels of isoniazid in pharmaceutical formulation using silver nanoparticles decorated copolymer. Electrochim. Acta 188, 818–824.
Ratinac, K.R., Yang, W., Gooding, J.J., Thordarson, P., Braet, F., 2011. Graphene and related materials in electrochemical sensing. Electroanalysis 23 (4), 803–826.
Rawool, C.R., Srivastava, A.K., 2019. A dual template imprinted polymer modified electrochemical sensor based on Cu metal organic framework/mesoporous carbon for highly sensitive and selective recognition of rifampicin and isoniazid. Sens. Actuators B Chem. 288, 493–506.
Ren, F., Wang, H., Zhai, C., Zhu, M., Yue, R., Du, Y., Yang, P., Xu, J., Lu, W., 2014. Clean method for the synthesis of reduced graphene oxide-supported PtPd alloys with high electrocatalytic activity for ethanol oxidation in alkaline medium. ACS Appl. Mater. Interfaces 6 (5), 3607–3614.
Riahi, S., Mousavi, M.F., Bathaie, S.Z., Shamsipur, M., 2005. A novel potentiometric sensor for selective determination of theophylline: theoretical and practical investigations. Anal. Chim. Acta 548 (1), 192–198.
Rivas, G.A., Rubianes, M.D., Rodriguez, M.C., Ferreyra, N.F., Luque, G.L., Pedano, M.L., Miscoria, S.A., Parrado, C., 2007. Carbon nanotubes for electrochemical biosensing. Talanta 74 (3), 291–307.
Rozwarski, D.A., Grant, G.A., Barton, D.H., Jacobs, W.R., Sacchettini, J.C., 1998. Modification of the NADH of the isoniazid target (InhA) from Mycobacterium tuberculosis. Science 279 (5347), 98–102.
Rubianes, M.a.D., Rivas, G.A., 2003. Carbon nanotubes paste electrode. Electrochem. Commun. 5 (8), 689–694.
Rubin, R.L., 2005. Drug-induced lupus. Toxicology 209 (2), 135–147.
Ryoo, R., Joo, S.H., Jun, S., 1999. Synthesis of highly ordered carbon molecular sieves via template-mediated structural transformation. J. Phys. Chem. B 103 (37), 7743–7746.
Safavi, A., Bagheri, M., 2008. Design of an optical sensor for indirect determination of isoniazid. Mol. Biomol. Spectrosc. 70 (4), 735–739.
Salimi, A., Kavosi, B., Fathi, F., Hallaj, R., 2013. Highly sensitive immunosensing of prostate-specific antigen based on ionic liquid–carbon nanotubes modified electrode: application as cancer biomarker for prostatebiopsies. Biosens. Bioelectron. 42, 439–446.
SANDERS, W.E., 1976. Drugs five years later: rifampin. Ann. Intern. Med. 85 (1), 82–86.
Santhanalkshmi, J., Rajesh, K., 2018. Fabrication of SnO2–graphene nanocomposite based electrode for sensitive monitoring of anti–Tuberculosis in human fluids. New J. Chem. 42, 2903–2915.
Satyanarayana, M., Reddy, K.K., Gobi, K.V., 2014. Multiwall carbon nanotube ensembled biopolymer electrode for selective determination of isoniazid in vitro. Anal. Methods 6 (11), 3772–3778.
Sensi, P., 1983. History of the development of rifampin. Rev. Infect. Dis. 5 (Suppl. ment_3), S402–S406.
Sepehri, Z., Bagheri, H., Ranjbari, E., Amiri-Aref, M., Amidi, S., Rouini, M.R., Ardakani, Y.H., 2017. Simultaneous electrochemical determination of isoniazid and ethambutol using poly-melamine/electrodeposited gold nanoparticles modified pre-anodized glassy carbon electrode. Ionics 1–11.
Shabani, R., Lakhaiy Rizi, Z., Moosavi, R., 2018. Selective potentiometric sensor for isoniazid ultra-trace determination based on Fe3O4 nanoparticles modified carbon paste electrode (Fe3O4/CPE). Int. J. Nanosci. Nanotechnol. 14 (3), 241–249.
Shah, M.H., Stewart, J.T., 1983. Amperometric determination of isoniazid in a flowing stream at the glassy carbon electrode. Anal. Lett. 16 (12), 913–923.
Shah, P., Pandya, T., Gohel, M., Thakkar, V., 2019. Development and Validation of HPLC method for simultaneous estimation of Rifampicin and Ofloxacin using experimental design. J. Taibah Univ. Sci. 13 (1), 146–154.
Shahrokhian, S., Amiri, M., 2007. Multi-walled carbon nanotube paste electrode for selective voltammetric detection of isoniazid. Microchim. Acta 157 (3–4), 149–158.
Shahrokhian, S., Asadian, E., 2010. Simultaneous voltammetric determination of ascorbic acid, acetaminophen and isoniazid using thionine immobilized multi-walled carbon nanotube modified carbon paste electrode. Electrochim. Acta 55 (3), 666–672.
Shane, A.L., 2006. Red Book: 2006 Report of the Committee on Infectious Diseases.
Shao, Y., Wang, J., Wu, H., Liu, J., Aksay, I.A., Lin, Y., 2010. Graphene based electrochemical sensors and biosensors: a review. Electroanalysis 22 (10), 1027–1036.
Shetty, D.N., Narayana, B., Samshuddin, S., 2012. Novel Reagents for the Spectrophotometric Determination of Isoniazid. ISRN Spectroscopy, 2012.
Shewiyo, D., Kaale, E., Risha, P., Dejaegher, B., Smeyers-Verbeke, J., Vander Heyden, Y., 2012. Optimization of a reversed-phase-high-performance thin-layer chromatography method for the separation of isoniazid, ethambutol, rifampicin and pyrazinamide in fixed-dose combination antituberculosis tablets. J. Chromatogr. A 1260, 232–238.
Shiri, S., Pajouheshpoor, N., Khoshsafar, H., Amidi, S., Bagheri, H., 2017. An electrochemical sensor for the simultaneous determination of rifampicin and isoniazid using a C-dots@ CuFe 2 O 4 nanocomposite modified carbon paste electrode. New J. Chem. 41 (24), 15564–15573.
Si, X., Jiang, L., Wang, X., Ding, Y., Luo, L., 2015. Determination of isoniazid content via cysteic acid/graphene modified glassy carbon electrode. Anal. Methods 7 (2), 793–798.
Simic, M.G., Jovanovic, S.V., 1989. Antioxidation mechanisms of uric acid. J. Am. Chem. Soc. 111 (15), 5778–5782.
Song, Z., Lü, J., Zhao, T.J.T., 2001. Chemiluminescence sensor for isoniazid with controlled-reagent-release technology. Talanta 53 (6), 1171–1177.
Song, H., Zhang, L., Su, Y., Lv, Y., 2017. Recent advances in graphitic carbon nitride-based chemiluminescence, cataluminescence and electrochemiluminescence. J. Anal. Test. 1 (4), 274–290.
Sonkar, P.K., Yadav, M., Prakash, K., Ganesan, V., Sankar, M., Yadav, D.K., Gupta, R., 2018. Electrochemical sensing of rifampicin in pharmaceutical samples using meso-tetrakis (4-hydroxyphenyl) porphyrinato cobalt (II) anchored carbon nanotubes. J. Appl. Electrochem. 48 (8), 937–946.
Spindola, R.F., Zanin, H., Macena, C.S., Contin, A., Luz, R.d.C.S., Damos, F.S., 2017. Evaluation of a novel composite based on functionalized multi-walled carbon nanotube and iron phthalocyanine for electroanalytical determination of isoniazid. J. Solid State Electrochem. 21 (4), 1089–1099.
Stankovich, S., Dikin, D.A., Piner, R.D., Kohlhaas, K.A., Kleinhammes, A., Jia, Y., Wu, Y., Nguyen, S.T., Ruoff, R.S., 2007. Synthesis of graphene-based nanosheets via chemical reduction of exfoliated graphite oxide. Carbon 45 (7), 1558–1565.
Stets, S., Tavares, T.M., Peralta-Zamora, P.G., Pessoa, C.A., Nagata, N., 2013. Simultaneous determination of rifampicinand isoniazid in urineand pharmaceutical formulations by multivariate visible spectrophotometry. J. Braz. Chem. Soc. 24 (7), 1198–1205.
Stockley, I.H., 1994. Anticoagulant Drug Interactions.
Suarez, J., Ranguelova, K., Jarzecki, A.A., Manzerova, J., Krymov, V., Zhao, X., Yu, S., Metlitsky, L., Gerfen, G.J., Magliozzo, R.S., 2009. An oxyferrous heme/protein-based radical intermediate is catalytically competent in the catalase reaction of Mycobacterium tuberculosis catalase-peroxidase (KatG). J. Biol. Chem. 284 (11), 7017–7029.
Sun, X., Jia, M., Guan, L., Ji, J., Zhang, Y., Tang, L., Li, Z., 2015. Multilayer graphene–gold nanocomposite modified stem-loop DNA biosensor for peanut allergen-Ara h1 detection. Food Chem. 172, 335–342.

Swamy, N., Basavaiah, K., Vinay, K.B., 2015. Titrimetric assay of isoniazid with perchloric acid in non-aqueous medium. J. Anal. Chem. 70 (6), 696–699.
Swamy, N., Basavaiah, K., Vamsikrishna, P., 2018. Research article stability-indicating UV-spectrophotometric assay of rifampicin. Insight Pharmaceut. Sci. 8 (1), 1–12.
Szlósarczyk, M., Piech, R., Bator, B., Maślanka, A., Opoka, W., Krzek, J., 2012. Voltammetric determination of isoniazid using cyclic renewable mercury film silver based electrode. Pharm. Anal. Acta 3, 5.
Tabrizi, M.A., Tavakkoli, A., Dhand, V., Rhee, K.Y., Park, S.-J., 2014. Eco-friendly one-pot synthesis of gold decorated reduced graphene oxide using beer as a reducing agent. J. Ind. Eng. Chem. 20 (6), 4327–4331.
Tafazoli, S., Mashregi, M., O'brien, P.J., 2008. Role of hydrazine in isoniazid-induced hepatotoxicity in a hepatocyte inflammation model. Toxicol. Appl. Pharmacol. 229 (1), 94–101.
Thapliyal, N., Karpoormath, R.V., Goyal, R.N., 2015. Electroanalysis of antitubercular drugs in pharmaceutical dosage forms and biological fluids: a review. Anal. Chim. Acta 853, 59–76.
Torrent, J., Izquierdo, I., Cabezas, R., Jané, F., 1989. Theophylline-isoniazid interaction. Drug Intell. Clin. Pharm. 23 (2), 143–145.
Ty, E., Moran, E., Cooke, F., 2016. Oxford Handbook of Infectious Diseases and Microbiology. Oxford University Press.
Tyszczuk, K., 2008. Application of an in situ plated lead film electrode to the analysis of testosterone by adsorptive stripping voltammetry. Anal. Bioanal. Chem. 390 (7), 1951–1956.
Tyszczuk, K., Korolczuk, M., 2009. New protocol for determination of rifampicine by adsorptive stripping voltammetry. Electroanalysis 21 (1), 101–106.
Varner, T.R., Bookstaver, P.B., Rudisill, C.N., Albrecht, H., 2011. Role of rifampin-based combination therapy for severe community-acquired Legionella pneumophila pneumonia. Ann. Pharmacother. 45 (7–8), 967–976.
Vu, D., Koster, R., Bolhuis, M., Greijdanus, B., Altena, R., Nguyen, D., Brouwers, J., Uges, D., Alffenaar, J., 2014. Simultaneous determination of rifampicin, clarithromycin and their metabolites in dried blood spots using LC–MS/MS. Talanta 121, 9–17.
Wang, J., 1992. Injection analysis—from flow-injection analysis to batch-injection analysis. Microchem. J. 45 (2), 219–224.
Wang, J., 2005. Carbon-nanotube based electrochemical biosensors: a review. Electroanalysis 17 (1), 7–14.
Wang, J., Taha, Z., 1991. Batch injection analysis. Anal. Chem. 63 (10), 1053–1056.
Wang, C., Liu, Q., Shao, X., Hu, X., 2007. Voltammetric determination of dopamine in human serum and urine at a glassy carbon electrode modified by cysteic acid based on electrochemical oxidation of l-cysteine. Anal. Lett. 40 (4), 689–704.
Wang, G., Yang, J., Park, J., Gou, X., Wang, B., Liu, H., Yao, J., 2008. Facile synthesis and characterization of graphene nanosheets. J. Phys. Chem. C 112 (22), 8192–8195.
Wang, H., Cai, C., Chu, C., Liu, J., Kong, Y., Zhu, M., Zhang, T., 2012. A simple and rapid HPLC/UV method for simultaneous quantification of four constituents in anti-tuberculosis 4-FDC tablets by pre-column derivatization. Asian J. Pharm. Sci. 7 (4), 303–309.
Wei, C.-J., Lei, B., Musser, J.M., Tu, S.-C., 2003. Isoniazid activation defects in recombinant Mycobacterium tuberculosis catalase-peroxidase (KatG) mutants evident in InhA inhibitor production. Antimicrob. Agents Chemother. 47 (2), 670–675.
Winder, F., Collins, P., 1970. Inhibition by isoniazid of synthesis of mycolic acids in Mycobacterium tuberculosis. Microbiology 63 (1), 41–48.
Xiong, Y., Zhou, H., Zhang, Z., He, D., He, C., Spectroscopy, B., 2007. Flow-injection chemiluminescence sensor for determination of isoniazid in urine sample based on molecularly imprinted polymer. Spectrochim. Acta A Mol. Biomol. Spectrosc. 66 (2), 341–346.
Yan, H., Xiao, H., Xie, Q., Liu, J., Sun, L., Zhou, Y., Zhang, Y., Chao, L., Chen, C., Yao, S., 2015. Simultaneous electroanalysis of isoniazid and uric acid at poly (sulfosalicylic acid)/electroreduced carboxylated graphene modified glassy carbon electrode. Sens. Actuators B Chem. 207, 167–176.
Yang, G., Wang, C., Zhang, R., Wang, C., Qu, Q., Hu, X., 2008. Poly (amidosulfonic acid) modified glassy carbon electrode for determination of isoniazid in pharmaceuticals. Bioelectrochemistry 73 (1), 37–42.
Yao, H., Sun, Y., Lin, X., Tang, Y., Liu, A., Li, G., Li, W., Zhang, S., 2007. Selective determination of epinephrine in the presence of ascorbic acid and uric acid by electrocatalytic oxidation at poly (eriochrome black T) film-modified glassy carbon electrode. Anal. Sci. 23 (6), 677–682.
Yao, Z., Zhu, M., Jiang, F., Du, Y., Wang, C., Yang, P., 2012. Highly efficient electrocatalytic performance based on Pt nanoflowers modified reduced graphene oxide/carbon cloth electrode. J. Mater. Chem. 22 (27), 13707–13713.
Yao, Z., Yue, R., Zhai, C., Jiang, F., Wang, H., Du, Y., Wang, C., Yang, P., 2013. Electrochemical layer-by-layer fabrication of a novel three-dimensional Pt/graphene/carbon fiber electrode and its improved catalytic performance for methanol electrooxidation in alkaline medium. Int. J. Hydrogen Energy 38 (15), 6368–6376.
YU, A.-M., SUN, D.-M., GU, H.-Y., CHEN, H.-Y., 1996. Catalytic oxidation of ascorbic acid at a polyhistidine modified electrode and its application to the voltammetric resolution of ascorbic acid and dopamine. Anal. Lett. 29 (15), 2633–2643.
Yu, H., Jian, X., Jin, J., Wang, F., Wang, Y., Qi, G.-c., 2013. Preparation of hybrid cobalt–iron hexacyanoferrate nanoparticles modified multi-walled carbon nanotubes composite electrode and its application. J. Electroanal. Chem. 700, 47–53.
Yun Xia, H., Ya Hu, X., 2005. Determination of isoniazid using a gold electrode by differential pulse voltammetry. Anal. Lett. 38 (9), 1405–1414.
Zare, H.R., Nasirizadeh, N., Chatraei, F., Makarem, S., 2009. Electrochemical behavior of an indenedione derivative electrodeposited on a renewable sol–gel derived carbon ceramic electrode modified with multi-wall carbon nanotubes: application for electrocatalytic determination of hydrazine. Electrochim. Acta 54 (10), 2828–2836.
Zargar, B., Hatamie, A., Spectroscopy, B., 2013. Localized surface plasmon resonance of gold nanoparticles as colorimetric probes for determination of Isoniazid in pharmacological formulation. Spectrochim. Acta A Mol. Biomol. Spectrosc. 106, 185–189.
Zhang, Z., Yin, J., 2014. Sensitive detection of uric acid on partially electro-reduced graphene oxide modified electrodes. Electrochim. Acta 119, 32–37.
Zhang, F., Wang, X., Ai, S., Sun, Z., Wan, Q., Zhu, Z., Xian, Y., Jin, L., Yamamoto, K., 2004. Immobilization of uricase on ZnO nanorods for a reagentless uric acid biosensor. Anal. Chim. Acta 519 (2), 155–160.
Zhang, H., Wu, L., Li, Q., Du, X., 2008. Determination of isoniazid among pharmaceutical samples and the patients' saliva samples by using potassium ferricyanide as spectroscopic probe reagent. Anal. Chim. Acta 628 (1), 67–72.
Zhang, F., Gu, S., Ding, Y., Li, L., Liu, X., 2013. Simultaneous determination of ofloxacin and gatifloxacin on cysteic acid modified electrode in the presence of sodium dodecyl benzene sulfonate. Bioelectrochemistry 89, 42–49.
Zhang, F., Gu, S., Ding, Y., Zhou, L., Zhang, Z., Li, L., 2013. Electrooxidation and determination of cefotaxime on Au nanoparticles/poly (L-arginine) modified carbon paste electrode. J. Electroanal. Chem. 698, 25–30.
Zhang, Y., Bo, X., Nsabimana, A., Luhana, C., Wang, G., Wang, H., Li, M., Guo, L., 2014. Fabrication of 2D ordered mesoporous carbon nitride and its use as electrochemical sensing platform for H2O2, nitrobenzene, and NADH detection. Biosens. Bioelectron. 53, 250–256.
Zheng, D., Ye, J., Zhou, L., Zhang, Y., Yu, C., 2009. Simultaneous determination of dopamine, ascorbic acid and uric acid on ordered mesoporous carbon/Nafion composite film. J. Electroanal. Chem. 625 (1), 82–87.
Zhou, Z., Chen, L., Liu, P., Shen, M., Zou, F., 2010. Simultaneous determination of isoniazid, pyrazinamide, rifampicin and acetylisoniazid in human plasma by high-performance liquid chromatography. Anal. Sci. 26 (11), 1133–1138.
Zhou, X., Zhang, J., Wu, H., Yang, H., Zhang, J., Guo, S., 2011. Reducing graphene oxide via hydroxylamine: a simple and efficient route to graphene. J. Phys. Chem. C 115 (24), 11957–11961.
Zhou, Z., Wu, X., Wei, Q., Liu, Y., Liu, P., Ma, A., Zou, F., 2013. Development and validation of a hydrophilic interaction liquid chromatography–tandem mass spectrometry method for the simultaneous determination of five first-line antituberculosis drugs in plasma. Anal. Bioanal. Chem. 405 (19), 6323–6335.
Zhu, X., Xu, J., Duan, X., Lu, L., Zhang, K., Yu, Y., Xing, H., Gao, Y., Dong, L., Sun, H., 2015. Controlled synthesis of partially reduced graphene oxide: enhance electrochemical determination of isoniazid with high sensitivity and stability. J. Electroanal. Chem. 757, 183–191.
Zou, J., Huang, L.-L., Jiang, X.-Y., Jiao, F.-P., Yu, J.-G., 2018. Electrochemical behaviors and determination of rifampicin on graphene nanoplatelets modified glassy carbon electrode in sulfuric acid solution. Desalin. Water Treat. 120, 272–281.